Electronic Supplementary Information for

# Palladium-Catalyzed Oxidative Homocoupling of Pyrazole Boronic Esters to Access Versatile Bipyrazoles and the Flexible Metal–Organic Framework Co(4,4′-bipyrazolate)

Mercedes Taylor,[†,◊,‡] Martin Juhl,[⊥] Dasol Hwang,[⊥] Gul Barg Hadaf,[⊥] Ever Velasquez,[§,‡] Julia Oktawiec,[◊] Jonathan B. Lefton,[§] Tomce Runcevski,[§] Jeffrey R. Long,[◊,‡,§]* Ji-Woong Lee[⊥]*

[†]Center for Integrated Nanotechnologies, Sandia National Laboratories, Albuquerque, New Mexico 87185, United States

[⊥] Department of Chemistry & Nano-Science Center, University of Copenhagen, Copenhagen 2100, Denmark

[§]Department of Chemical and Biomolecular Engineering, University of California, Berkeley, California 94720, United States

[◊]Department of Chemistry, University of California, Berkeley, California 94720, United States

[§]Department of Chemistry, Southern Methodist University, Texas 75205, United States

[‡]Materials Sciences Division, Lawrence Berkeley National Laboratory, Berkeley, California 94720, United States

## Table of Contents

## General Methods

All chemicals, unless stated otherwise, were purchased from commercial suppliers and used without further purification. Solvents used were HPLC grade. Analytical thin layer chromatography was done on Merck DC-Alufolien $SIO_2$ 60 F254 0.2 mm thick pre-coated TLC plates. Column chromatography was performed using $SiO_2$ from ROCC (SI 1721, 60 Å, 40-63 µm). $^1H$ and $^{13}C$ NMR spectra were recorded with 500 MHz Ultrashield Plus 500 spectrometer and 126 MHz on a Bruker. $^1H$ and $^{13}C$ NMR were also recorded at 500 MHz and 125 MHz on a Bruker Avance 3 spectrometer with a BBFO probe. All chemical shifts ($\delta$) are given in ppm and all coupling constants ($J$) in Hertz (Hz). The following abbreviations are used for multiplicity for NMR resonances: s = singlet, d = doublet, t = triplet, q = quartet and m = multiplet.

## General Procedure for Homocoupling of Pyrazole Boronic Esters (Scheme S1)

An 8 mL vial fitted with a stirring bar was charged with the pyrazole boronic ester (1 mmol), $Pd(PPh_3)_4$ (58 mg, 0.050 mmol, 5 mol%), $Cs_2CO_3$ (326 mg, 1.00 mmol, 1 equiv), dioxane (0.5 mL) and $H_2O$ (0.5 mL) in that order. The vial was closed with a screw seal containing a septum. The reaction was fitted with a balloon filled with air and stirred (1000 rpm) for 18 h at 95 °C. The reaction mixture was transferred to a separatory funnel. $H_2O$ (20 mL) was added and the aqueous phase was extracted with $CH_2Cl_2$ (3×20 mL). The organic fractions were combined and dried over $MgSO_4$, filtered and concentrated *in vacuo* and subjected to further purification.
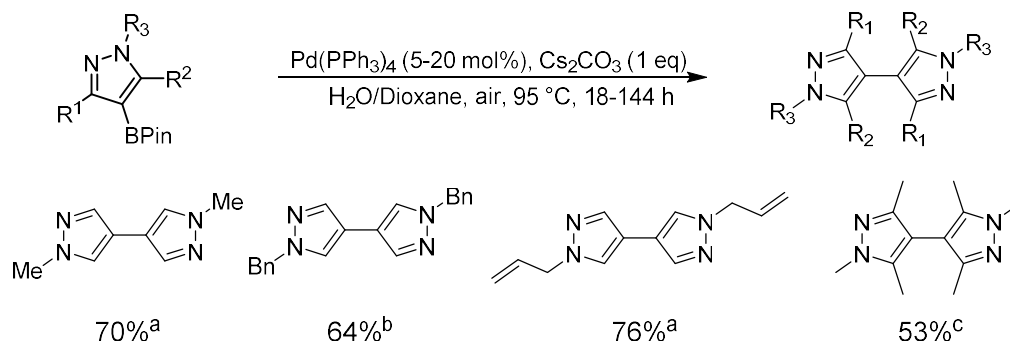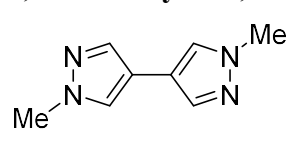


**Scheme S1.** Substrate scope of optimized pyrazoleboronic ester homocoupling, with isolated yields. Conditions for 1 mmol substrate: (a) $Pd(PPh_3)_4$ (5 mol%), 18 h; (b) $Pd(PPh_3)_4$ (10 mol%), 18 h; (c), $Pd(PPh_3)_4$ (20 mol%), 144 h.

**1,1′-dimethyl-1*H*,1′*H*-4,4′-bipyrazole (2a).** The starting material 1-methylpyrazole-4-boronic acid pinacol ester (208 mg, 1.00 mmol) was used in the general procedure described above, and the product was purified by flash column chromatography using ethyl acetate (EtOAc) → 20% MeOH in EtOAc as eluent. The title compound was obtained as a white powder, (57 mg, 70%). $^1H$ NMR (500 MHz, CDCl$_3$). $\delta$ = 7.55 (s, 2H), 7.43 (s, 2H), 3.92 (s, 6H). $^{13}C$ NMR (125 MHz, CDCl$_3$). $\delta$ = 137.0, 126.7, 114.3, 39.1. HRMS

C$_8$H$_{11}$N$_4$ [M+H]+; calculated 163.0978, found 163.0994. $^1$H and $^{13}$C NMR spectra are provided in Figure S1.

**1$H$,1′$H$-4,4′-bipyrazole (2b).** In a 50 mL round bottom flask equipped with a magnetic stirring bar and a reflux condenser, 1-(tetrahydro-2$H$-pyran-2-yl)-1$H$-pyrazole-4-boronic acid pinacol ester (1.0 g, 3.6 mmol), Pd(PPh$_3$)$_4$ (0.63 g, 15 mol), and Cs$_2$CO$_3$ (1.2 g, 3.6 mmol, 1 equiv) were dissolved in water and 1,4-dioxane (1:1, v/v, 5 mL). The solution was heated to 100 °C under air and refluxed for 24 h. After full conversion (by TLC, diethylether and heptane (1:10), stained with KMnO$_4$), the black crude solution was dissolved in $N,N$-dimethylformamide (DMF) (100 mL), then filtered to remove palladium black and other insoluble impurities. A solution of 1.6 M HCl in diethylether (25 mL) was added to the reaction mixture. The mixture was stirred overnight at room temperature and concentrated under reduced pressure, then dissolved in CH$_2$Cl$_2$ (100 mL). A white precipitation was observed, which was filtered affording a gray powder after washing with CH$_2$Cl$_2$ twice. The powder was further concentrated under reduced pressure to afford the bipyrazole as a gray powder, (196 mg, 81%). $^1$H NMR (500 MHz, $d$-DMSO). δ =7.85 (s). $^{13}$C NMR (126 MHz, $d$-DMSO). δ =130.9, 113.3. HRMS C$_6$H$_7$N$_4$ [M+H]+; calculated 135.0665, found 135.0678. $^1$H and $^{13}$C NMR spectra are provided in Figure S2. To further confirm the identity of the compound, the HCl salt was obtained and subjected to elemental analysis, with the results as follows: Calculated for C$_6$H$_8$Cl$_2$N$_4$: C, 34.8; H, 3.89; N, 27.06, found: C, 36.99; H, 4.64; N, 27.63. In further confirmation of the reaction procedure, methylation of **2b** afforded the soluble variant **1,1′-dimethyl-1$H$,1′$H$-4,4′-bipyrazole** in good isolated yield and purity (see below).

**1,1′-dimethyl-1$H$,1′$H$-4,4′-bipyrazole: Methylation of 1$H$,1′$H$-4,4′-bipyrazole**

An 8 mL vial fitted with a stirring bar was charged with 1,1'-dimethyl-1$H$,1'$H$-4,4'-bipyrazole (20.0 mg, 0.149 mmol), K$_2$CO$_3$ (247 mg, 1.79 mmol, 12 equiv), DMF (1 mL) and methyl iodide (211 mg, 1.49 mmol, 10 equiv) in that order. The mixture was stirred at room temperature for 5 days. The mixture was then transferred to a separatory funnel, and water (25 mL) was added. The product was extracted with CH$_2$Cl$_2$ (3x15mL). The organic fractions were combined and dried over MgSO$_4$, filtered and concentrated *in vacuo*. The mixture was subjected to flash column chromatography using EtOAc → 20% MeOH in EtOAc as eluent. The title compound was obtained as a white powder, (19 mg, 79%). Spectral data is in accordance with the previously reported.

**1,1 ′-dibenzyl-1$H$,1′$H$-4,4′-bipyrazole.** The starting material 1-benzylpyrazole-4-boronic acid pinacol ester (284 mg, 1.00 mmol) was used in the general procedure described above, using 10 mol% Pd(PPh$_4$). The product was purified by flash column chromatography using 1:1 EtOAc/heptane eluent. The title compound was obtained as a white powder, (101 mg, 64%). $^1$H NMR (500 MHz, CDCl$_3$). δ = 7.60 (s, 2H), 7.42 (s, 2H), 7.37-7.30 (m, 6H), 7.23 (d, $J$ = 7 Hz, 4H), 5.29 (s, 4H). $^{13}$C NMR (126 MHz, CDCl$_3$). δ = 137.2, 136.6, 129.0, 128.3, 127.8, 125.8, 114.6, 56.3. HRMS C$_{20}$H$_{19}$N$_4$ [M+H]+; calculated 315.1604, found 315.1606. $^1$H and $^{13}$C NMR spectra are provided in Figure S3.

**1,1′-diallyl-1$H$,1′$H$-4,4′-bipyrazole.** The starting material 1-allylpyrazole-4-boronic acid pinacol ester (234 mg, 1 mmol) was used in the general procedure described above, and the product was purified by flash column chromatography using 1:1 → 4:1 EtOAc/heptane as eluent. The title compound was obtained as a yellow oil, (81 mg, 76%). $^1$H NMR (500 MHz, CDCl$_3$). $\delta$ = 7.59 (d, $J$ = 0.6 Hz, 2H), 7.47 (d, $J$ = 0.5 Hz, 2H), 6.04 (ddt, $J$ = 17.0, 10.2, 6.0 Hz, 2H), 5.26 (ddq, $J$ = 23.2, 17.1, 1.4 Hz, 4H), 4.74 (dt, $J$ = 6.0, 1.4 Hz, 4H. $^{13}$C NMR (126 MHz, CDCl$_3$). $\delta$ = 137.2, 133.0, 125.6, 118.9, 114.4, 54.9. HRMS C$_{12}$H$_{15}$N$_4$ [M+H]+; calculated 215.1291, found 215.1295. $^1$H and $^{13}$C NMR spectra are provided in Figure S4.
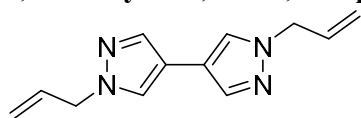
**1,1′,3,3′,5,5′-hexamethyl-1$H$,1′$H$-4,4′-bipyrazole.** The starting material 1-methylpyrazole-4-boronic acid pinacol ester (208 mg, 1.00 mmol) was used following the general procedure described above, with 20 mol% Pd(PPh$_4$) and a reaction time of 6 d. The product was purified by flash column chromatography using toluene → 10% EtOH in toluene as eluent. Impurities of triphenylphosphine oxide were still present in the mixture. The mixture was dissolved in EtOAc (20 mL) and transferred to a separatory funnel. The product was extracted with 1 M HCl$_{aq}$ (3×20 mL). The fractions where combined and the solution was basified with 5 M NaOH$_{aq}$. The mixture was transferred to a separatory funnel and the product was extracted with EtOAc (3×20 mL). The organic fractions were combined and dried over MgSO$_4$, filtered, and concentrated *in vacuo* to afford the title compound as a clear oil, (58 mg, 53%). $^1$H NMR (500 MHz, CDCl$_3$). $\delta$ = 3.80 (s, 6H), 2.06 (s, 6H), 2.05 (s, 6H). HRMS C$_{12}$H$_{19}$N$_4$ [M+H]+; calculated 219.1604, found 219.1622. $^1$H and $^{13}$C NMR spectra are provided in Figure S5.
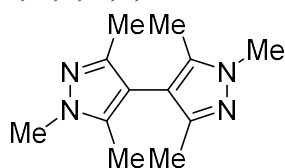
**Co(bpz).** H$_2$bpz (0.62 g, 4.6 mmol, 1.3 equiv) and Co(SO$_3$CF$_3$)$_2$ (1.24 g, 3.47 mmol, 1 equiv) were combined in anhydrous $N$,$N$-diethylformamide (DEF, 14.3 mL) in a 50-mL solvent bomb under air. The mixture was degassed over 5 freeze–pump–thaw cycles, then sealed by closing the stopcock of the solvent bomb while the frozen reaction mixture remained under vacuum. The solvent bomb was then heated at 160 °C for 3 d to afford a purple microcrystalline solid. The solvent bomb was subsequently opened to air, and anhydrous DMF (200 mL) was added to the solid product. The slurry was transferred to a Pyrex jar, sealed, and heated to 110 °C overnight. The supernatant was subsequently removed and replaced with 200 mL of fresh anhydrous DMF, and the slurry was again heated to 110 °C overnight. This solvent exchange procedure was performed once daily for 7 days to completely remove unreacted starting material from the pores. Subsequently, the DMF was replaced with anhydrous CH$_2$Cl$_2$ following the same procedure but without heating; these CH$_2$Cl$_2$ exchanges were performed once daily for 3 days to allow activation from a lower-boiling solvent. To activate the material, the CH$_2$Cl$_2$ was decanted until 25 mL of solution remained. The resultant slurry was transferred to a 100-mL Schlenk flask, and the CH$_2$Cl$_2$ was evaporated by flowing Ar at room temperature for 1 h. The resultant solid was dried by flowing Ar at 160 °C for 6 h, then placed under dynamic vacuum at 160 °C overnight to yield **Co(bpz)** (0.204 g, 1.07 mmol, 31%). Anal. Calcd. for C$_6$H$_4$N$_4$Co:

C, 37.72, H, 2.11, N, 29.32; found: C, 38.09, H, 2.28, N, 29.52. IR:1516 (m),1382 (m), 1260 (m), 1155 (m), 1046 (s), 1014 (m), 917 (s), 831 (s), 631 (s) cm−1. The desolvated solid was immediately transferred to a glovebox and handled under a dinitrogen atmosphere for all further experiments.

**Gas Adsorption**

Ultra-high purity (99.999% purity) $N_2$, $CO_2$, and $H_2$ were used for all adsorption measurements. Nitrogen, carbon dioxide, and hydrogen adsorption isotherms for pressures in the range of 0−1.1 bar were measured using a Micromeritics ASAP 2020 or 2420 gas adsorption analyzer. Activated samples were transferred under a $N_2$ atmosphere to preweighed analysis tubes, which were capped with a Transeal. Each sample was evacuated on the instrument until the outgas rate was less than 3 μbar/min. The evacuated analysis tube containing degassed sample was then carefully transferred to an electronic balance and weighed to determine the mass of sample (typically 30−50 mg). The tube was then fitted with an isothermal jacket and transferred back to the analysis port of the instrument. The outgas rate was again confirmed to be less than 3 μbar/min. Nitrogen and hydrogen adsorption isotherms were measured at 77 K using a liquid $N_2$ bath. Carbon dioxide adsorption isotherms were measured at 195 K using a solid $CO_2$/isopropanol bath. Adsorption isotherms for $N_2$, $CO_2$, and $H_2$ for Co(bpz) are provided in Figures S6-S10.

**Powder X-ray Diffraction**

Powder X-ray diffraction data for Co(bpz) was collected on Beamline 17-BM-B at the Advanced Photon Source at Argonne National Laboratory. Approximately 3 mg of fully desolvated framework was loaded into a 1.0 mm borosilicate capillary inside a $N_2$-filled glovebox. Each capillary was then attached to a custom designed gas-dosing cell equipped with a valve and transferred to the goniometer head. All adsorbed $N_2$ was then removed by evacuating *in situ* with a turbomolecular pump. An Oxford Cryosystems Cryostream 800 was used to maintain the temperature of the sample. Scattered intensity was measured by a PerkinElmer a-Si flat panel detector. The average wavelength of measurement was 0.45241 Å.

Powder X-ray diffraction data was collected for an activated sample of Co(bpz) under vacuum at 298 K and then at 433 K, and the crystal structures of activated Co(bpz) at 298 K and 433 K were solved from this data. The crystal structure solution process (including pattern visualization, pattern indexing, Pawley fitting, crystal structure solution and Rietveld refinement) was performed with the TOPAS 5 program suite.[1] The pattern indexing was done with the singular value decomposition method,[2] as implemented in TOPAS. Indexing provided a shortlist of unit cells with estimated parameters and crystal system symmetry. The parameters of the most probable unit cells were refined using Pawley structureless fitting.[3] A short list of possible space groups was obtained after close examination of the systematic absences of reflections in the powder patterns. Crystal structure solutions were initiated using the most probable space groups (*C*2/*c* for the pattern at 298 K, and *Ccc*2 for the pattern at 433 K). The crystal structure solution was performed by the global optimization method of simulated annealing in real space.[4] The ligand was

described in as a rigid body in Z-matrix notation. Due to the space group symmetry, the rigid body contained only one half of the ligand, whereas the remaining half was created as a symmetry equivalent of the asymmetric unit. During the simulated annealing runs, three rotations and three translations of the rigid body were set flexible, together with one fractional coordinate for the cobalt atom (the remaining fractional coordinates were fixed, as the cobalt atoms were found on special positions in both structures: 0, $y$, 0.25 for $C2/c$ and 0, 0.5, $z$ for $Ccc2$). Once a global minimum was reached, the crystal structures were subjected to Rietveld refinement,[5] in which all bond lengths and angles were refined within the rigid bodies, together with free refinement of all profile and lattice parameters. No restrains or constrains were used. All refinements converged quickly. The positions of the hydrogen atoms were calculated using the Mercury software suite.[6] The final Rietveld plots are presented in Figures S12 and S13 and the details of the refinement are given in Table S2.

After diffraction data was collected at 298 K and then at 433 K as described above, the sample was cooled down to 290 K quickly (at an approximate rate of 30 K/min), after which diffraction data was again collected. The 290 K diffraction data was subjected to Rietveld refinement[5], and this analysis indicated that 88% of the sample was now in the 298 K phase and 12% was in the 433 K phase. The fact that 88% of the sample reverted to the starting phase upon cooling indicates that the phase change is reversible; we hypothesize that had the cooling been performed more slowly and the sample allowed to reach equilibrium, it would eventually have returned to 100% in the 298 K phase. The reversibility of the temperature-induced phase change is further supported by the fact that prior to obtaining the original 298 K diffraction data, the sample had been heated to 433 K multiple times. Thus, because the original 298 K diffraction data does not show any of the 433 K phase is present, Co(bpz) is capable of fully reversing the heat-induced phase.

After the variable temperature studies, approximately 70 mbar of $CO_2$ gas was dosed to the sample using a custom-built gas dosing manifold at 290 K. The dose of gas was equilibrated on the sample for fifteen minutes, with no change in the pressure readout or diffraction patterns being observed at the end of this interval, and then the sample was slowly cooled down to 165 K at a rate of 2 K/min. Diffraction patterns collected every ten degrees were then analyzed further. A standard peak search, followed by indexing through the Single Value Decomposition approach,[2] as implemented in TOPAS-Academic,[7] enabled the determination of approximate unit-cell parameters. The unit cell dimensions of the $CO_2$-dosed phases were then obtained by Pawley refinement[3] and displayed a good fit to the data in all cases (Table S3; representative refinements are shown in Figures S14-S17). It should be noted that like other flexible materials with similar ligands, Co(bpz) has prominent asymmetric broadening of its peaks, as observed in many of the diffraction patterns measured during the apparent phases changes in this experiment.[8] This broadening contributes to the higher goodness-of-fit values observed in some cases. Additionally, at approximately 207 K, the pattern did not show an adequate fit to the $C2/c$ space group, despite fitting well at temperatures above and below. Instead, the diffraction pattern showed a duplication of the allowed reflections for $C2/c$, consistent with that of two $C2/c$ phases with similar unit cell parameters. As a result, a Pawley refinement incorporating two phases was undertaken and yielded reasonable goodness-of-fit parameters.

6

The unit cell parameters obtained through Pawley refinement provide a significant amount of information about the structural changes occurring in $CO_2$-dosed Co(bpz) upon cooling. First, the unit cell dimensions and volume of the 298 K structure under 70 mbar CO2 very closely match those of the 298 K structure under vacuum, given in Figure 1, indicating that the addition of 70 mbar $CO_2$ does not appreciably change the evacuated structure of Co(bpz).

Second, upon cooling from 298 K to 207 K, the unit cell volume of $CO_2$-dosed Co(bpz) gradually contracts, as shown in Figure 3 (bottom). This contraction is primarily associated with a decrease in the length of the crystallographic *b* axis and an increase in the length of the crystallographic *a* axis, leading to a vertical compression of the diamond-shaped channels apparent in Figure 1 that results in narrower channels. As the temperature cools and more $CO_2$ molecules adsorb into these channels, we hypothesize that this contraction accomplishes better contacts between the walls of the channels and the $CO_2$ molecules within the channels.

Third, the diffraction data obtained at 207 K could not be fit to a single set of unit cell parameters. Instead, this data was consistent with the presence of two distinct structural phases at this temperature, shown in Figure 3 (bottom) as open circles. The lesser-volume phase appears to be a continuation of the gradually contraction observed from 298 K to 207 K, but the greater-volume phase represents an abrupt expansion of the framework. This discrete phase change is consistent with the sharp step apparent in the $CO_2$ adsorption isotherm (Figure 2) and with the temperature-induced phase change depicted in Figure 4.

Finally, the abrupt unit cell expansion that occurs at 207 K is followed by a gradual increase in unit cell volume from 207 K to 165 K, as shown in Figure 3 (bottom). This gradual expansion is primarily associated with an increase in the length of the crystallographic *b* axis and a decrease in the length of the crystallographic *a* axis, and the unit cell parameters approach those of the expanded structure shown in Figure 4 (bottom). Thus, we hypothesize that after the discrete phase change at 207 K, the adsorption of additional $CO_2$ molecules gradually forces the framework to expand to accommodate more guest molecules.

The air stability of Co(bpz) was assessed by comparing its powder X-ray diffraction pattern immediately after synthesis to that obtained after exposure to air for one month (Figure S18). For this experiment, powder X-ray diffraction data were collected using Cu K$\alpha$ ($\lambda_{avg}$= 1.5418 Å) radiation with a Bruker AXS D8 Advance diffractometer with the generator set at 40 kV and 40 mA.

**Scanning Electron Microscopy**

Scanning electron microscopy (SEM) images of Co(bpz) were acquired using a Hitachi S-5000 SEM (imaged at 10 keV and 4 nA). The Co(bpz) samples for SEM imaging were not dried or activated before imaging. Samples were prepared by drop-casting particles in dichloromethane onto a silicone wafer, which was then sputter coated with a layer of gold

approximately 3 nm thick to reduce sample charging. The SEM data shows the as-synthesized Co(bpz) particles to be needle-shaped crystals approximately 1-4 μm in diameter and 10-20 μm in length. This morphology is consistent with the one-dimensional channels observed in the crystal structures of Co(bpz) (obtained from powder X-ray diffraction data), as well as with the SEM images of the extended analogue Co(bdp).[8]

**Table S1.** Synthesis optimization for methyl-substituted H$_2$bpz.
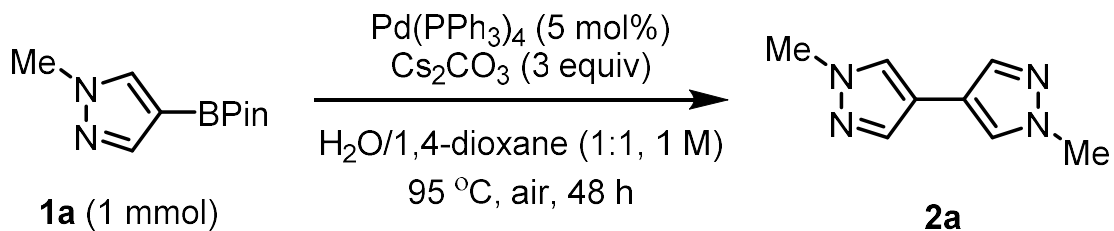


| Entry | Variation from above conditions | Conversion (%)[*] |
|-------|--------------------------------|-------------------|
| 1 | none | 85 |
| 2 | pure N$_2$ | 0 |
| 3 | pure O$_2$ | 30 |
| 4 | no base | 14 |
| 5 | K$_3$PO$_4$ instead of Cs$_2$CO$_3$ | 33 |
| 6 | Cs$_2$CO$_3$ (0.5 equiv) | 35 |
| 7 | Cs$_2$CO$_3$ (1 equiv) | 83 |
| 8 | LiCl additive (0.5 equiv) | 14 |
| 9 | only H$_2$O solvent | trace |
| 10 | only 1,4-dioxane solvent | 0 |
| 11 | H$_2$O/toluene | 23 |
| 12 | Pd(OAc)$_2$ | 12 |
| 13 | PdCl$_2$ and PPh$_3$ (20 mol%) | 32 |
| 14 | PdCl$_2$ and PCy$_3$ (20 mol%) | 11 |
| 15 | PdCl$_2$ and PPh$_3$ (20 mol%), CuI (2 equiv) | 78 |

[*]Conversion was determined by ^{1}H NMR spectroscopy.

**Table S2.** Experimental, unit cell, and refinement parameters obtained by Rietveld refinement using synchrotron X-ray powder diffraction patterns of activated Co(bpz) at 298 K and 433 K.

|  | Activated Co(bpz) | Activated Co(bpz) |
|---|---|---|
| $\lambda$ (Å) | 0.45118 | 0.45118 |
| Temperature | 298 K | 433 K |
| Space Group | $C2/c$ | $Ccc2$ |
| $a$ (Å) | 14.403(4) | 12.753(4) |
| $b$ (Å) | 10.664(2) | 12.526(4) |
| $c$ (Å) | 7.128(1) | 7.271(2) |
| $\beta$ (°) | 95.60(2) | 90 |
| $V$ (Å$^3$) | 1089.8(4) | 1161.6(6) |
| $R_{wp}$ (%) | 7.36 | 7.24 |
| $R_{exp}$ (%) | 0.45 | 0.14 |
| $R_p$ (%) | 4.92 | 5.37 |
| $R_{Bragg}$ (%) | 1.48 | 1.78 |

**Table S3.** Experimental, unit cell, and refinement parameters obtained by Pawley refinement using synchrotron X-ray powder diffraction patterns of Co(bpz) dosed with 70 mbar of $CO_2$ gas at 298 K before being cooled to 165 K.

| Temp. (K) | a (Å) | b (Å) | c (Å) | $\beta$ (º) | V (Å³) | $R_{wp}$ (%) |
|---|---|---|---|---|---|---|
| 298 | 14.289(4) | 10.693(4) | 7.1151(11) | 95.429(13) | 1082.4(5) | 5.12 |
| 288 | 14.374(3) | 10.585(3) | 7.1028(12) | 95.567(19) | 1075.6(4) | 4.75 |
| 277 | 14.465(3) | 10.464(3) | 7.0943(9) | 95.638(11) | 1068.7(4) | 4.96 |
| 267 | 14.562(3) | 10.308(3) | 7.0837(10) | 95.732(11) | 1058.0(4) | 5.24 |
| 257 | 14.668(4) | 10.144(3) | 7.0757(12) | 95.809(14) | 1047.4(4) | 5.79 |
| 247 | 14.758(5) | 9.954(3) | 7.0600(17) | 95.81(2) | 1031.8(5) | 6.21 |
| 237 | 14.861(5) | 9.810(3) | 7.0521(16) | 95.89(2) | 1022.7(5) | 6.95 |
| 227 | 14.914(5) | 9.711(3) | 7.0416(17) | 95.94(2) | 1014.4(5) | 7.42 |
| 217 | 14.935(6) | 9.657(4) | 7.034(2) | 95.96(2) | 1009.0(6) | 8.36 |
| 207 | 15.002(12) | 9.623(7) | 7.031(6) | 95.88(2) | 1009.6(14) | 3.86 |
| 207 | 14.545(14) | 10.376(8) | 7.057(9) | 95.72(11) | 1060.0(19) | 3.86 |
| 197 | 14.3232(16) | 10.6736(15) | 7.1452(8) | 95.148(11) | 1087.9(3) | 3.13 |
| 187 | 14.1153(13) | 10.9426(9) | 7.1791(4) | 95.025(5) | 1104.60(15) | 2.82 |
| 177 | 13.860(3) | 11.2581(17) | 7.2122(11) | 95.196(6) | 1120.8(3) | 3.2 |
| 165 | 13.683(5) | 11.472(4) | 7.226(3) | 95.610(10) | 1128.8(7) | 4.37 |

# Figures
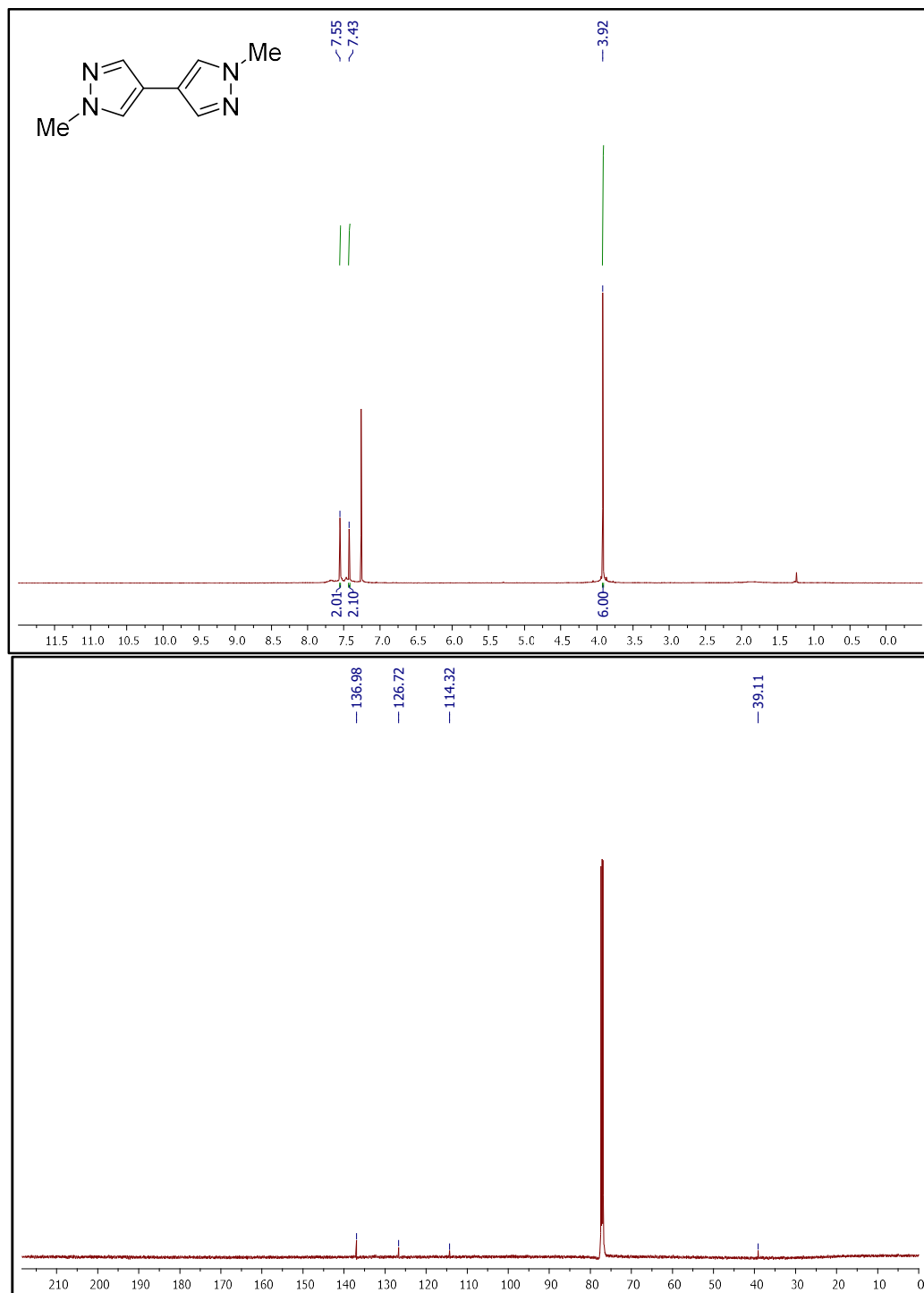


**Figure S1.** ^{1}H (top) and ^{13}C (bottom) NMR spectra for 1,1'-dimethyl-1*H*,1'*H*-4,4'-bipyrazole (**2a**).
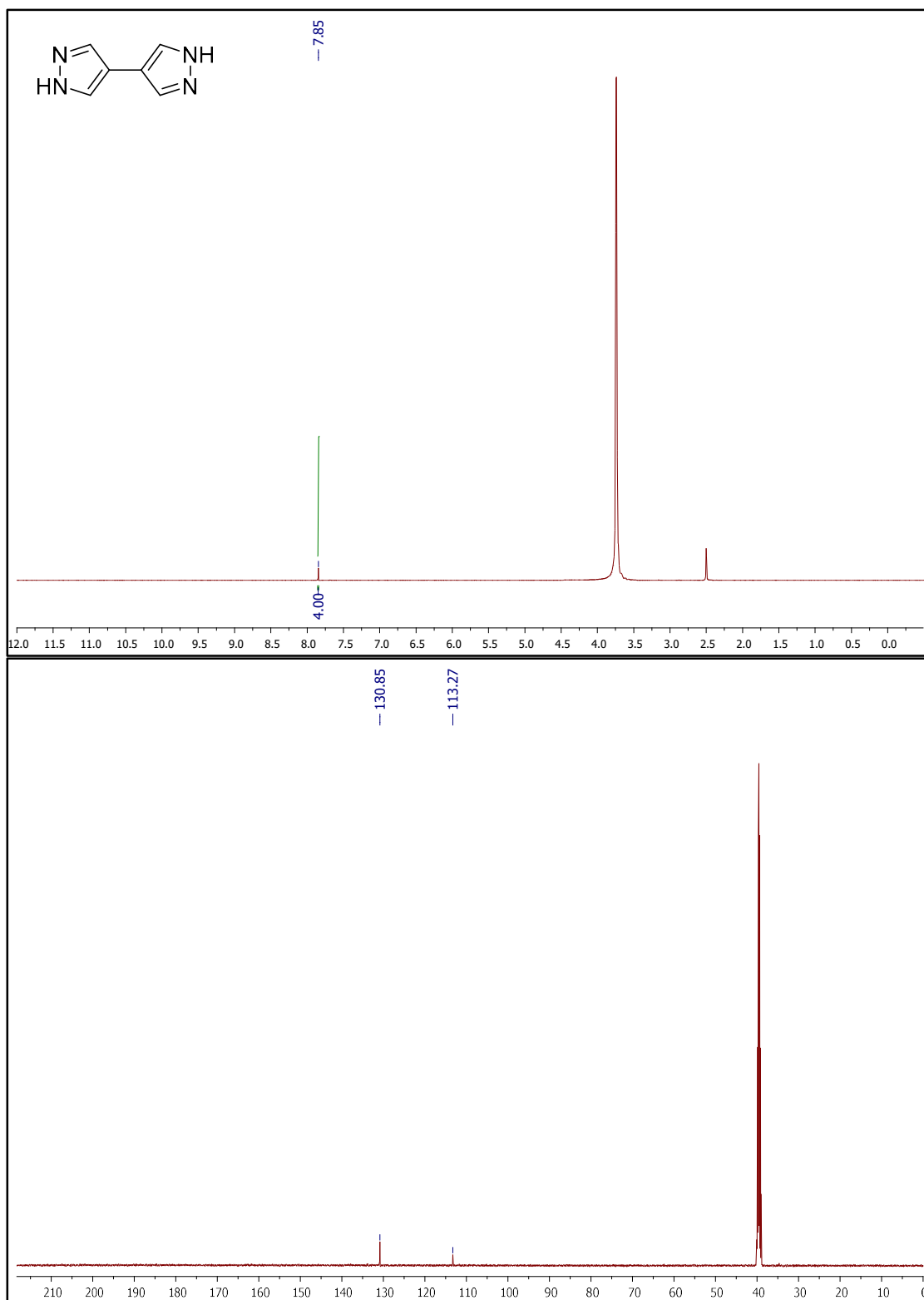
**Figure S2.** $^1$H (top) and $^{13}$C (bottom) NMR spectra for 1*H*,1'*H*-4,4'-bipyrazole (**2b**).
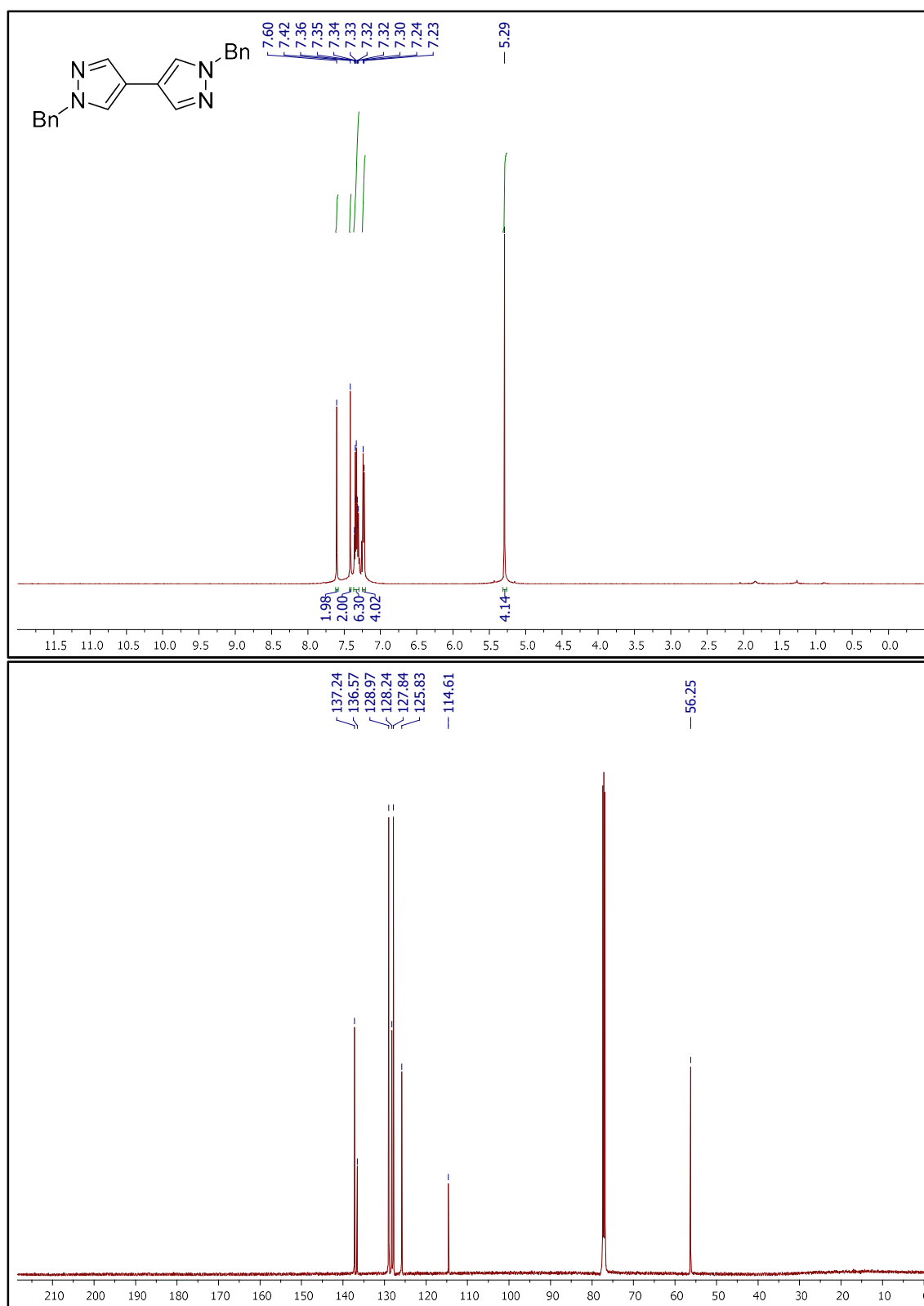
**Figure S3.** $^{1}$H (top) and $^{13}$C (bottom) NMR spectra for 1,1'-dibenzyl-1*H*,1'*H*-4,4'-bipyrazole.

14
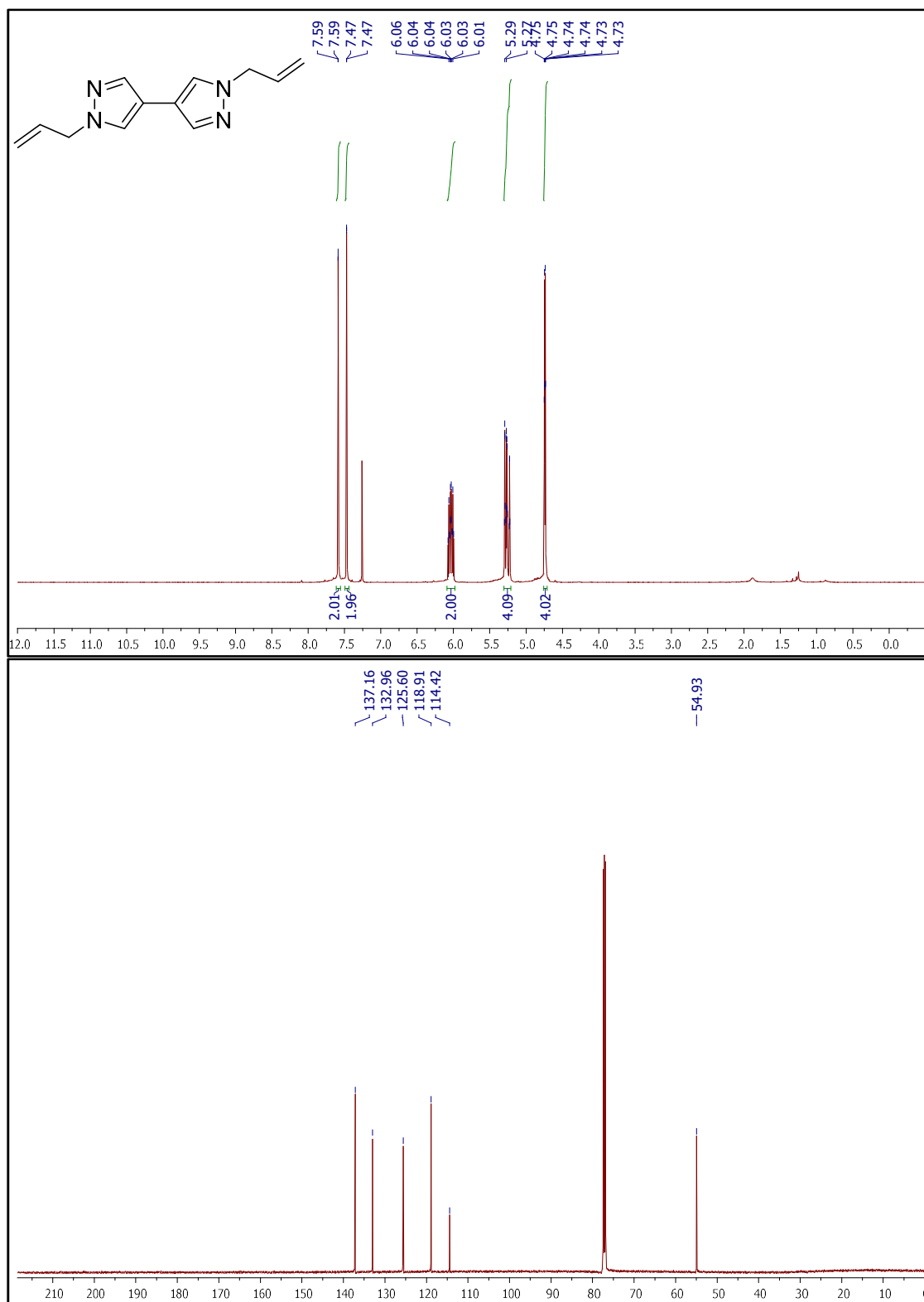
**Figure S4.** $^1$H (top) and $^{13}$C (bottom) NMR spectra for 1,1'-diallyl-1$H$,1'$H$-4,4'-bipyrazole.
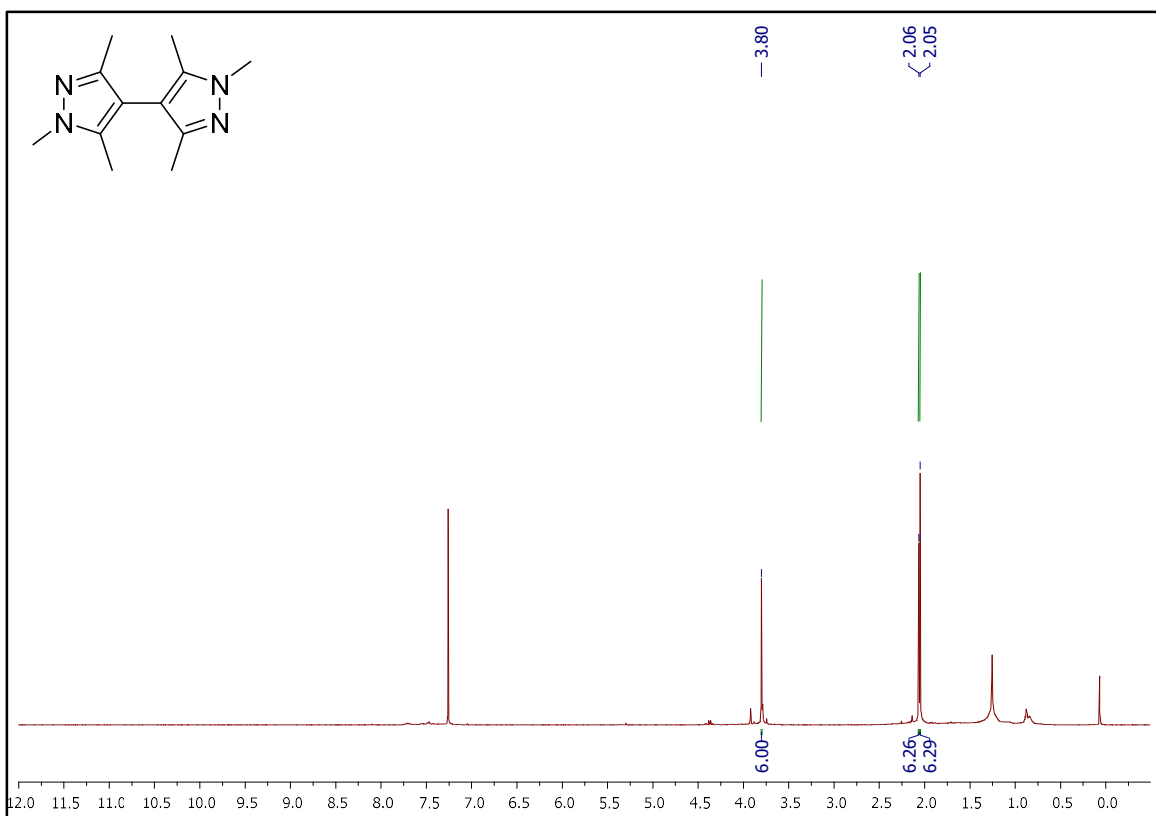
**Figure S5.** $^1$H NMR spectrum for 1,1',3,3',5,5'-hexamethyl-1$H$,1'$H$-4,4'-bipyrazole.
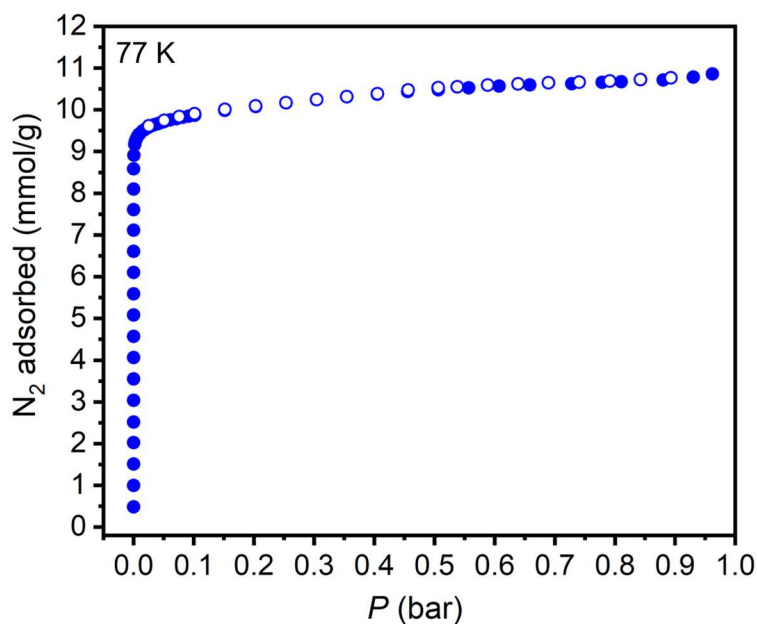
**Figure S6.** Low pressure $N_2$ adsorption isotherm for Co(bpz) at 77 K, plotted on a linear scale. Closed circles are adsorption and open circles are desorption.
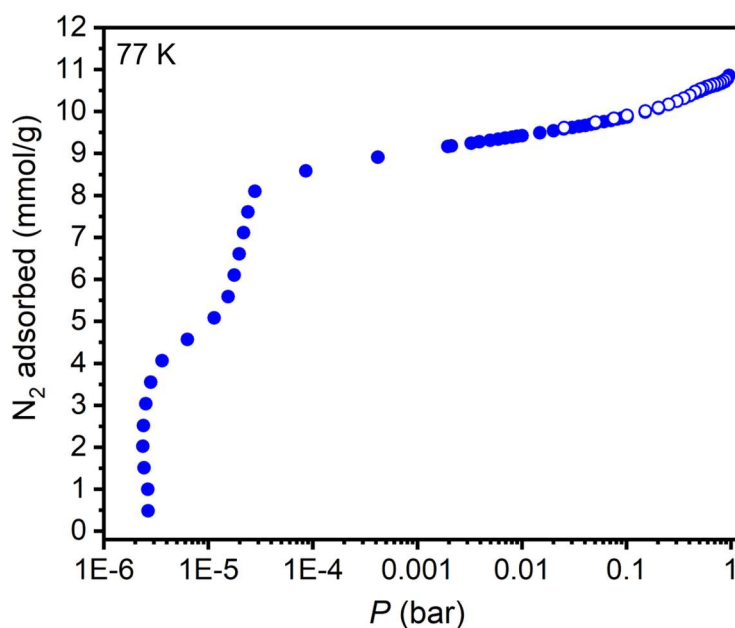


**Figure S7.** Low pressure $N_2$ adsorption isotherm for Co(bpz) at 77 K, plotted on a logarithmic scale. Closed circles are adsorption and open circles are desorption.
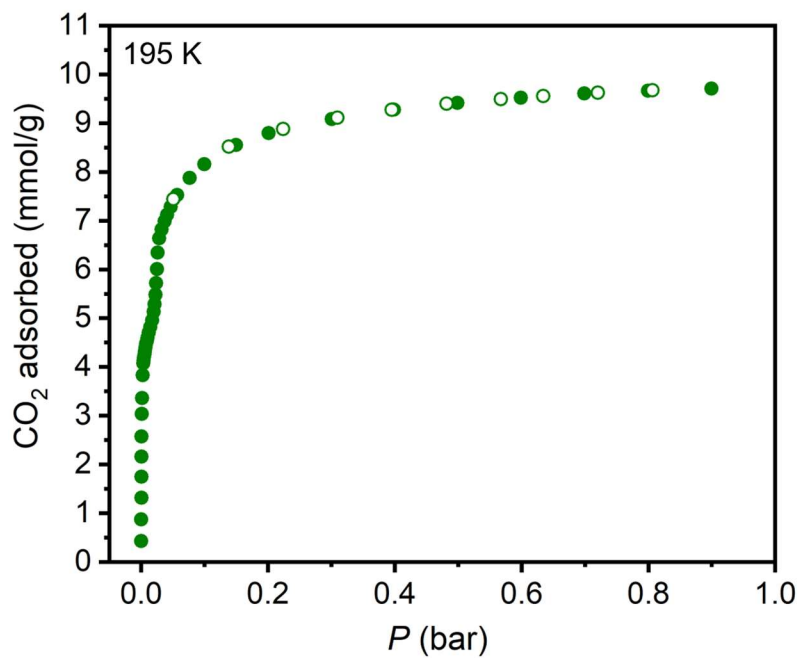
**Figure S8.** Low pressure $CO_2$ adsorption isotherm for Co(bpz) at 195 K, plotted on a linear scale. Closed circles are adsorption and open circles are desorption.



s
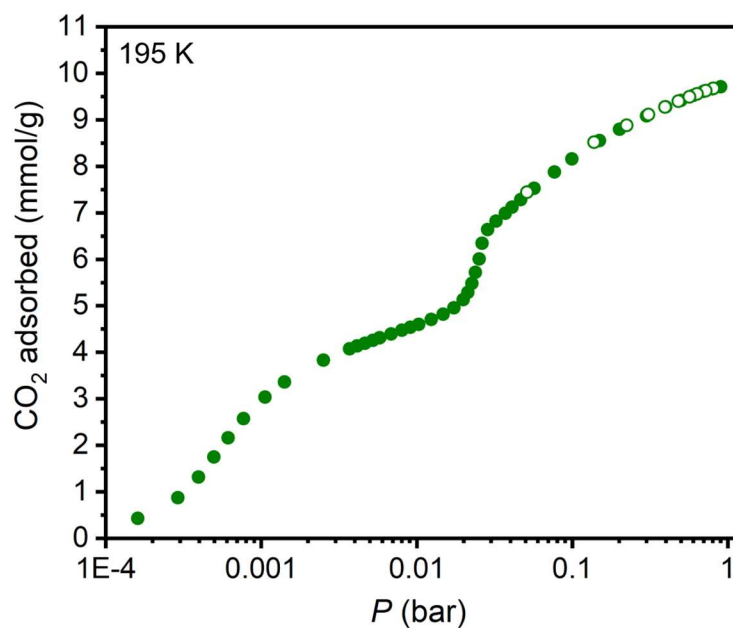
**Figure S9.** Low pressure $CO_2$ adsorption isotherm for Co(bpz) at 195 K, plotted on a logarithmic scale. Closed circles are adsorption and open circles are desorption.
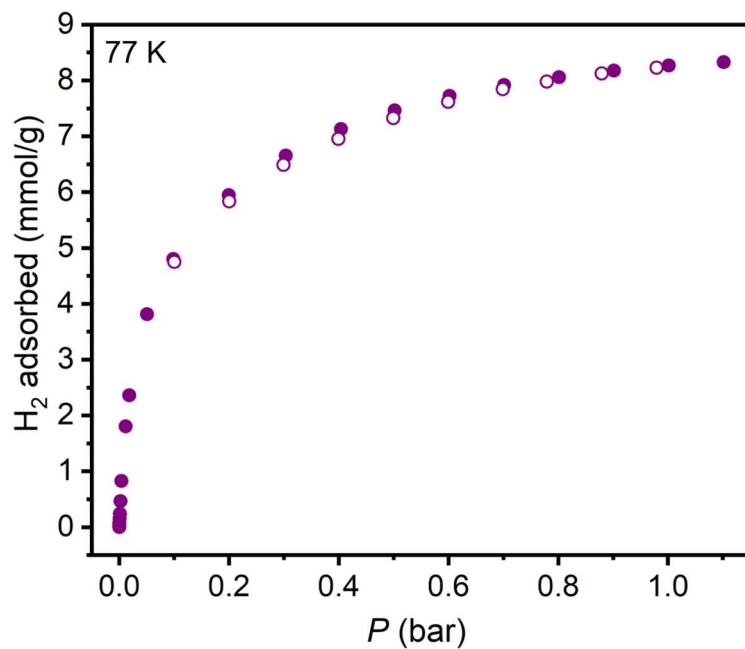
**Figure S10.** Low pressure $H_2$ adsorption isotherm for Co(bpz) at 77 K, plotted on a linear scale. Closed circles are adsorption and open circles are desorption.
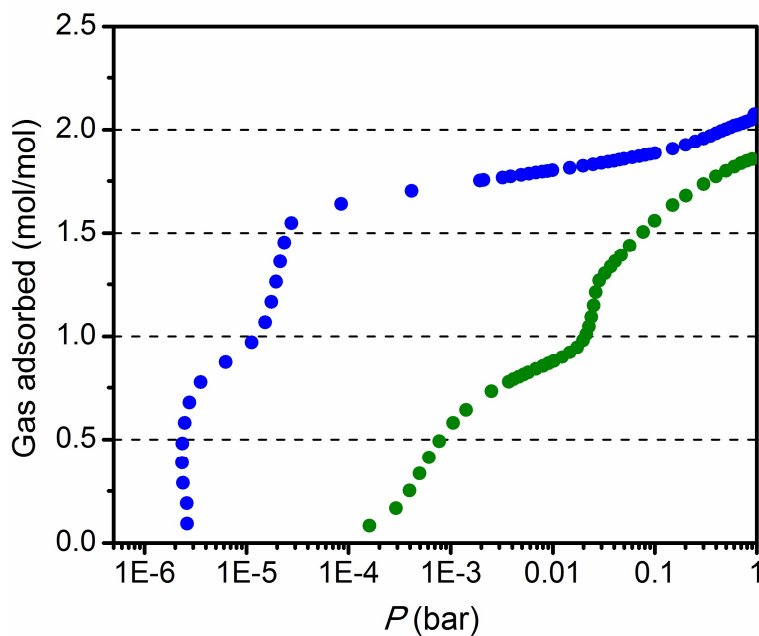


**Figure S11.** Low pressure $N_2$ at 77 K (blue) and $CO_2$ at 195 K (green) adsorption for Co(bpz), plotted on a logarithmic scale. For each gas, the first and second phases saturate at approximately 1 mol/mol and 2 mol/mol, respectively.
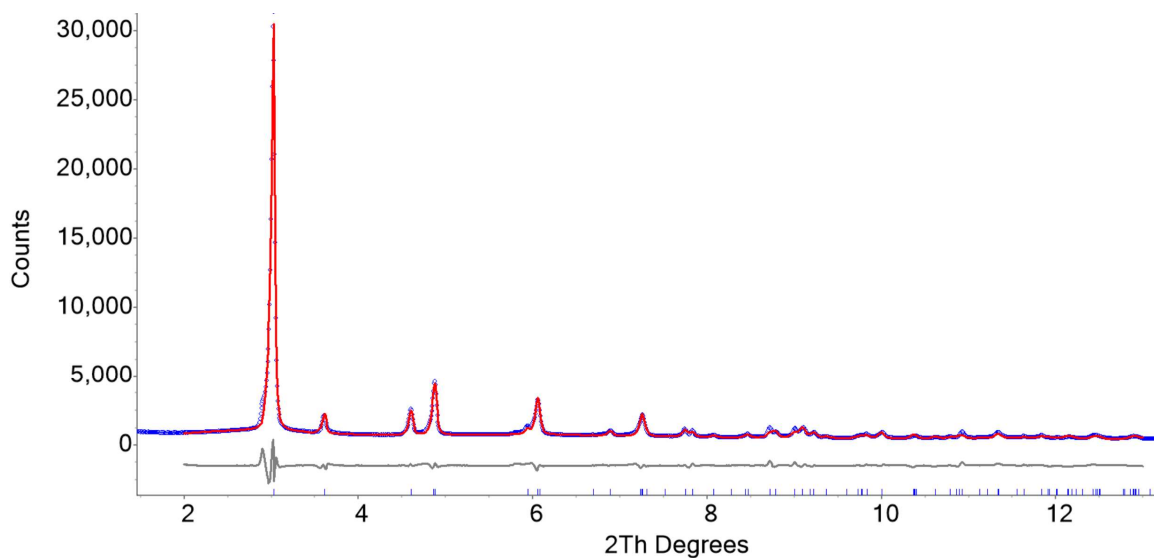
**Figure S12.** Rietveld refinement plot of the structure of activated Co(bpz) at 298 K. The observed X-ray scattered intensity is presented as blue dots, the simulated powder pattern as a red line, the difference curve as a gray line, and the Bragg reflections are presented as blue bars. Further details are given in Table S1.
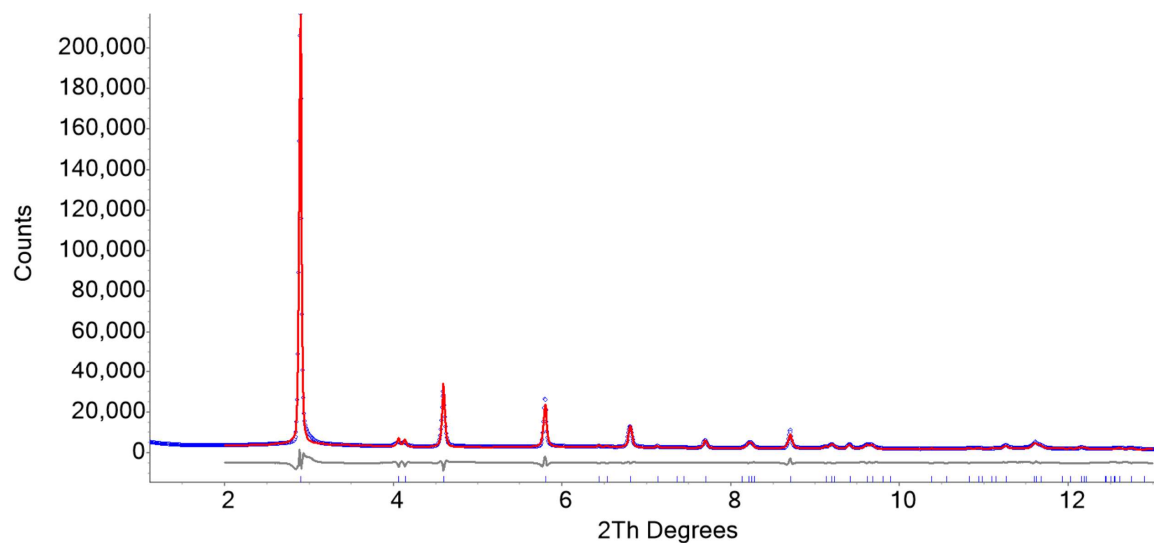


**Figure S13.** Rietveld refinement plot of the structure of activated Co(bpz) at 433 K. The observed X-ray scattered intensity is presented as blue dots, the simulated powder pattern as a red line, the difference curve as a gray line, and the Bragg reflections are presented as blue bars. Further details are given in Table S1.
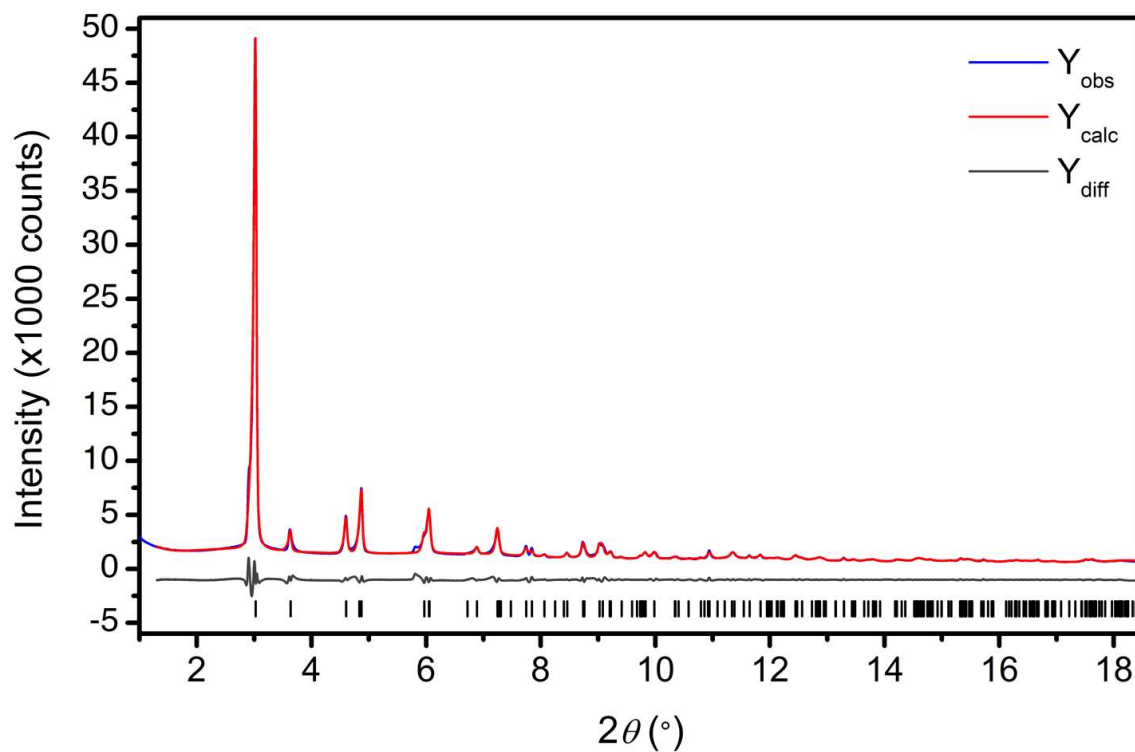
**Figure S14.** Pawley refinement of desolvated Co(bpz) under 70 mbar of $CO_2$ at 298 K from 1.0º to 18.5º. Blue and red lines represent the observed and calculated diffraction patterns, respectively. The gray line represents the difference between observed and calculated patterns, and the black tick marks indicate calculated Bragg peak positions.
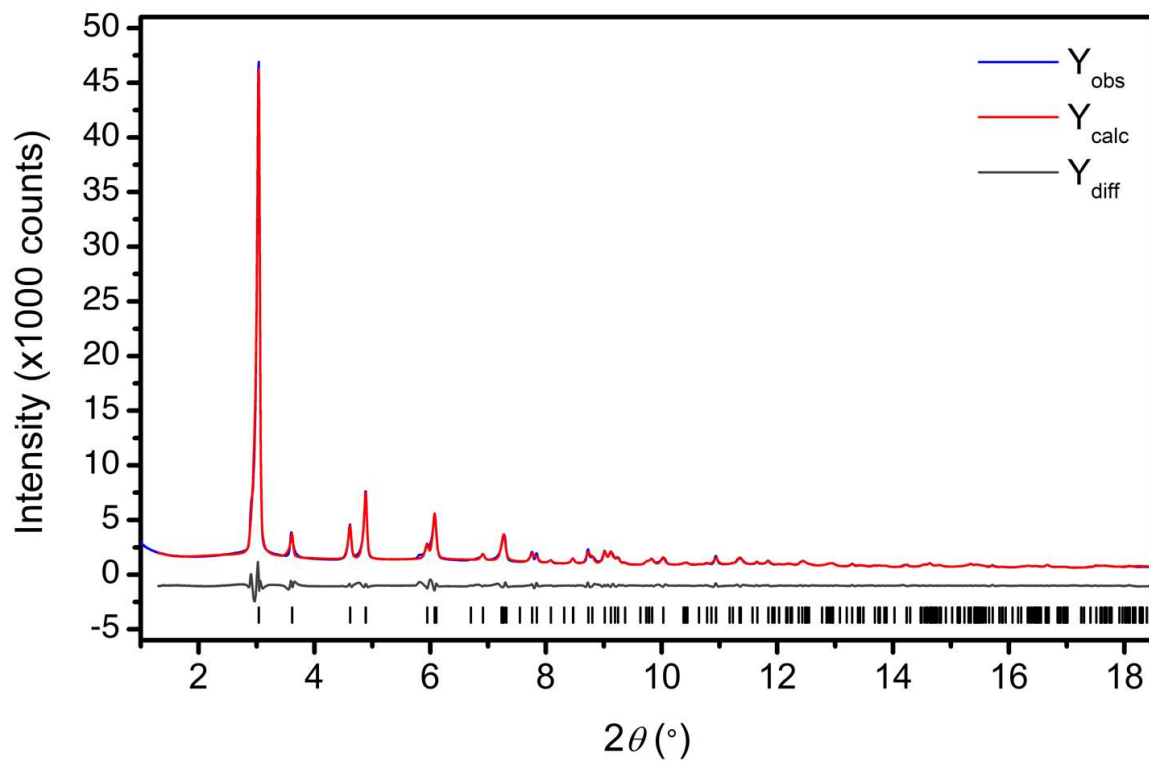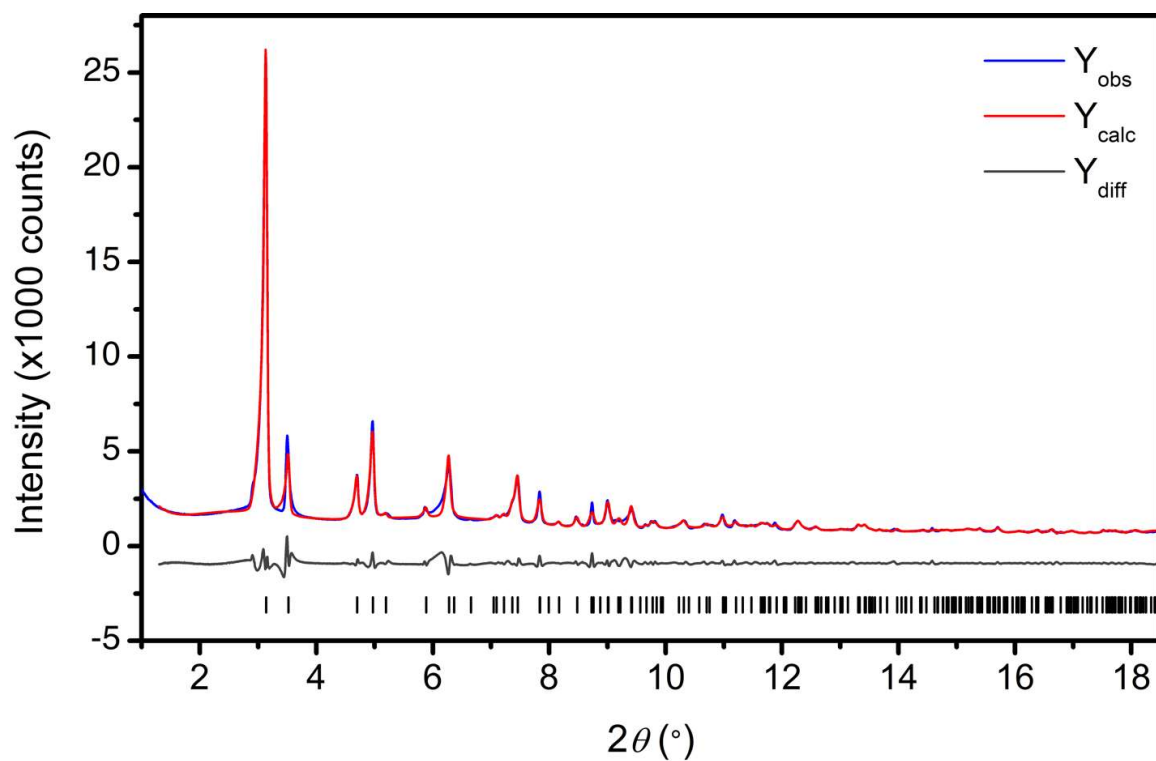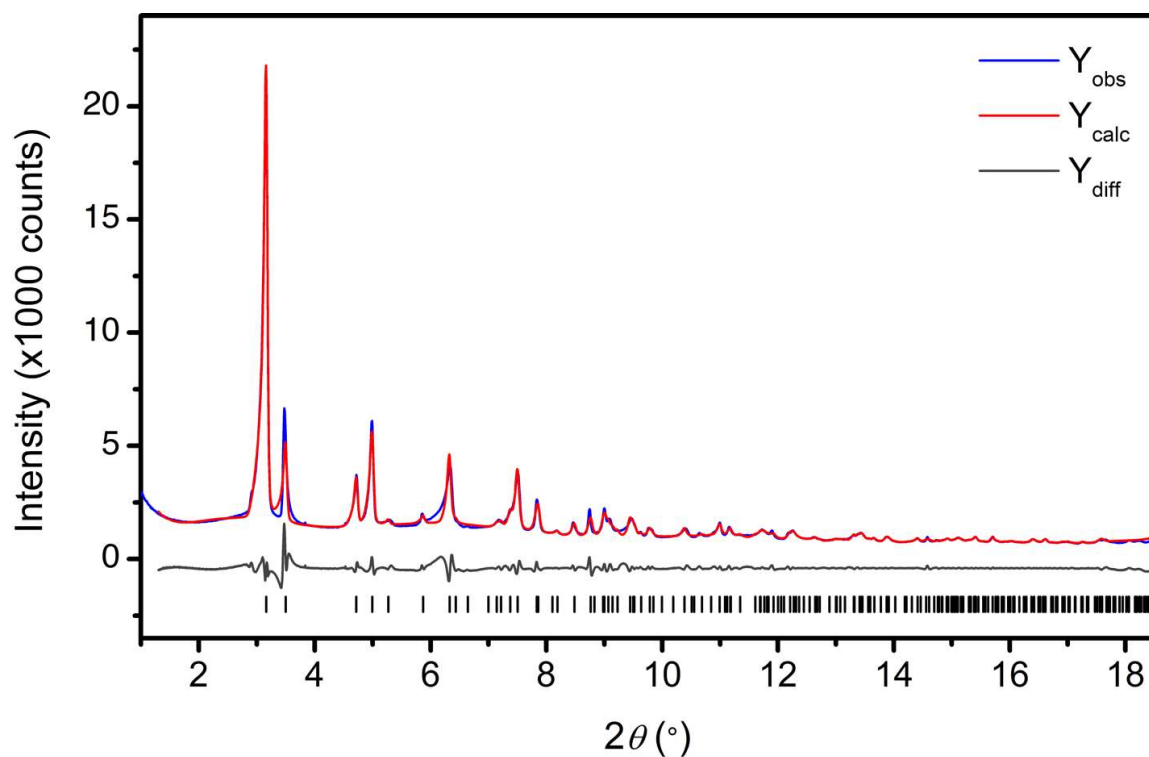
**Figure S15.** Pawley refinement of desolvated Co(bpz) under 70 mbar of $CO_2$ at 288 K from 1.0º to 18.5º. Blue and red lines represent the observed and calculated diffraction patterns, respectively. The gray line represents the difference between observed and calculated patterns, and the black tick marks indicate calculated Bragg peak positions.
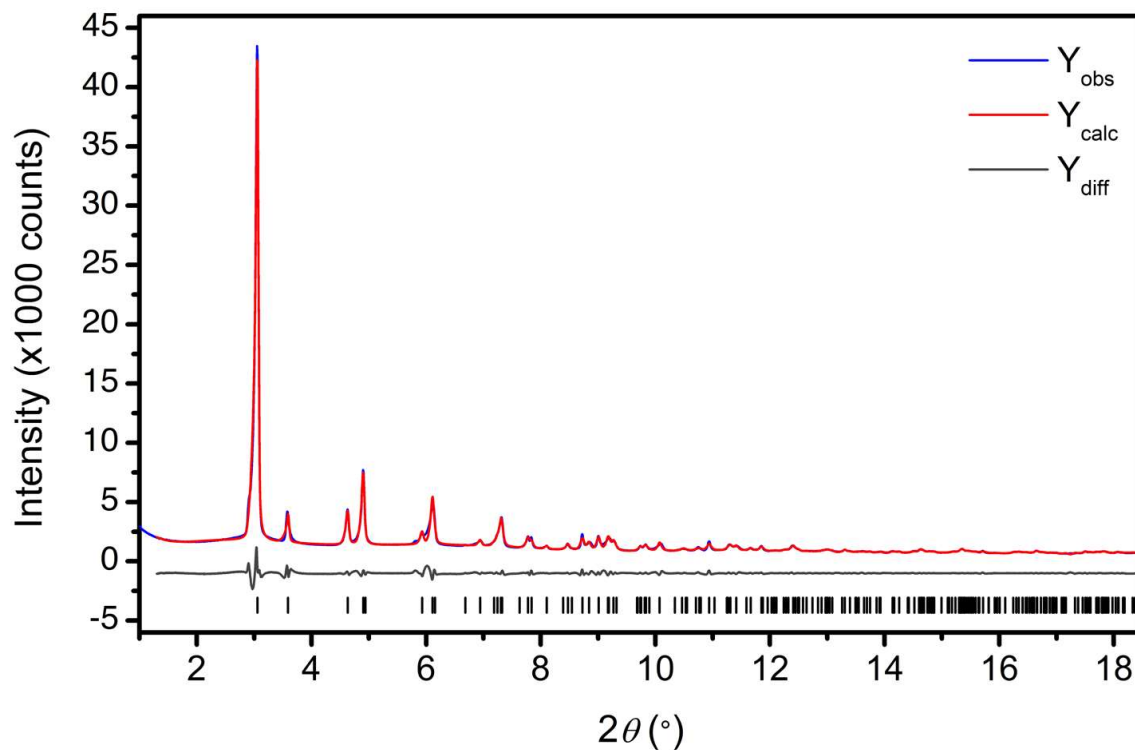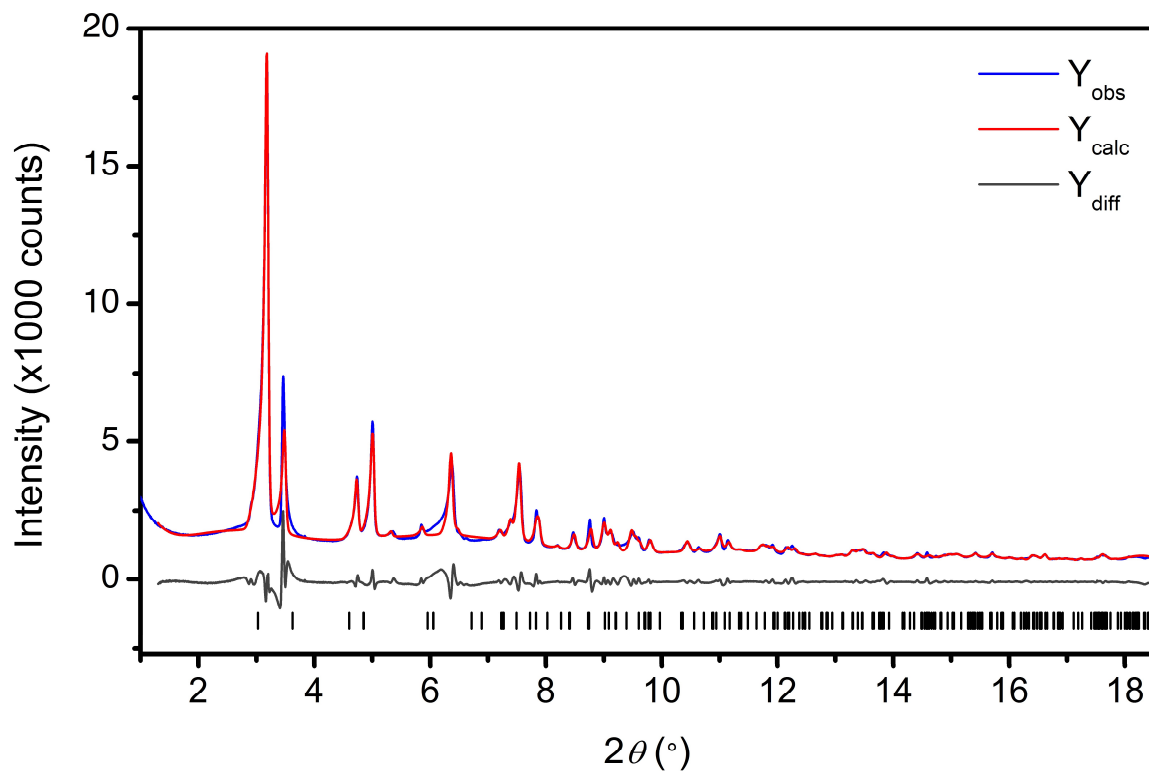
**Figure S16.** Pawley refinement of desolvated Co(bpz) under 70 mbar of $CO_2$ at 277 K from 1.0º to 18.5º. Blue and red lines represent the observed and calculated diffraction patterns, respectively. The gray line represents the difference between observed and calculated patterns, and the black tick marks indicate calculated Bragg peak positions.
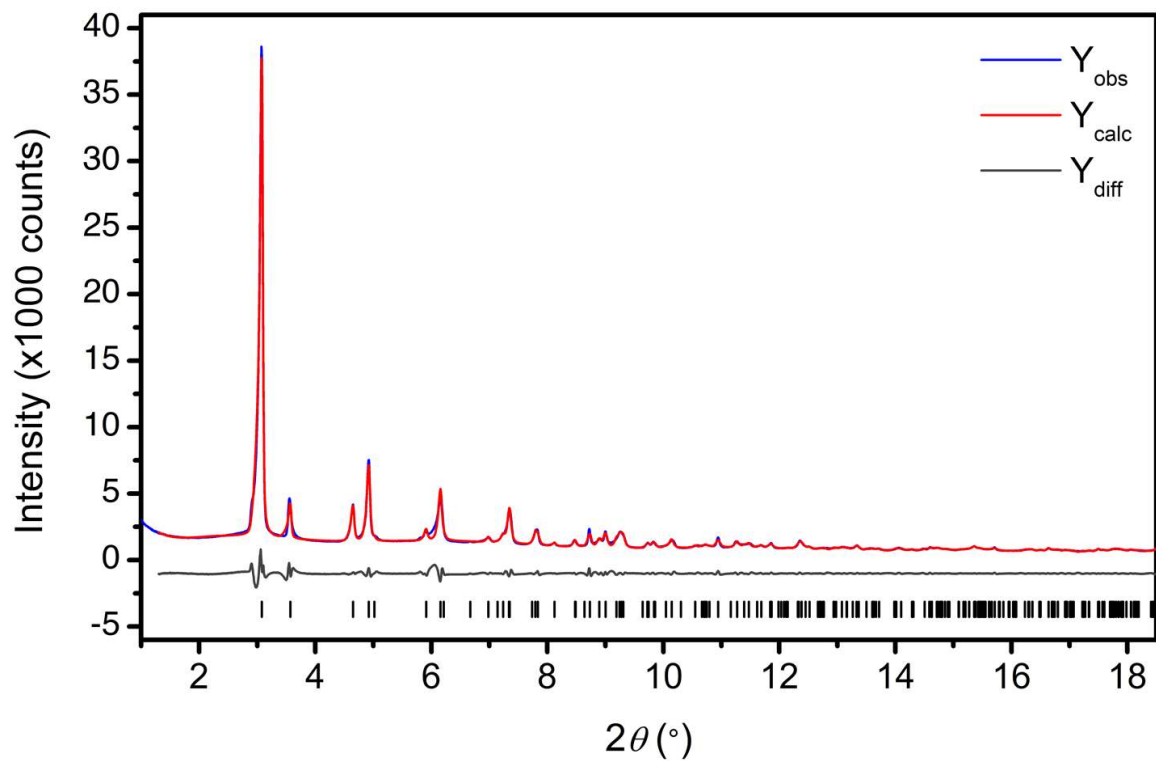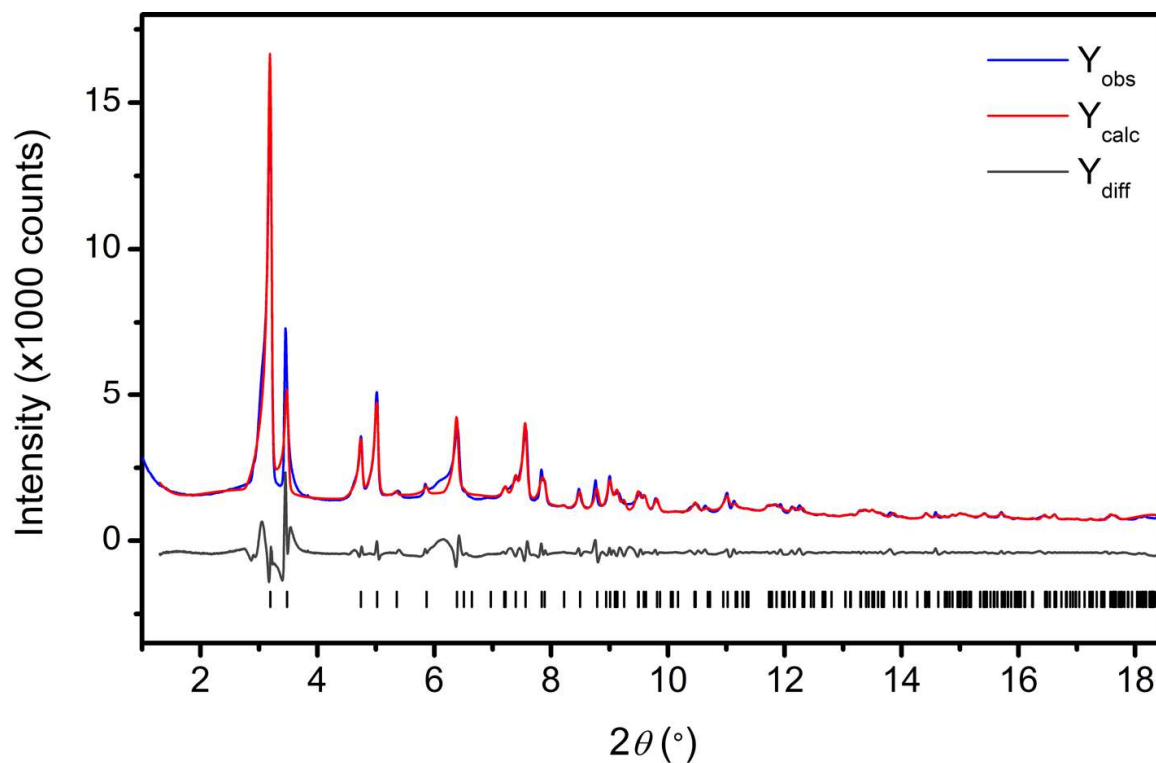
**Figure S17.** Pawley refinement of desolvated Co(bpz) under 70 mbar of $CO_2$ at 267 K from 1.0º to 18.5º. Blue and red lines represent the observed and calculated diffraction patterns, respectively. The gray line represents the difference between observed and calculated patterns, and the black tick marks indicate calculated Bragg peak positions.
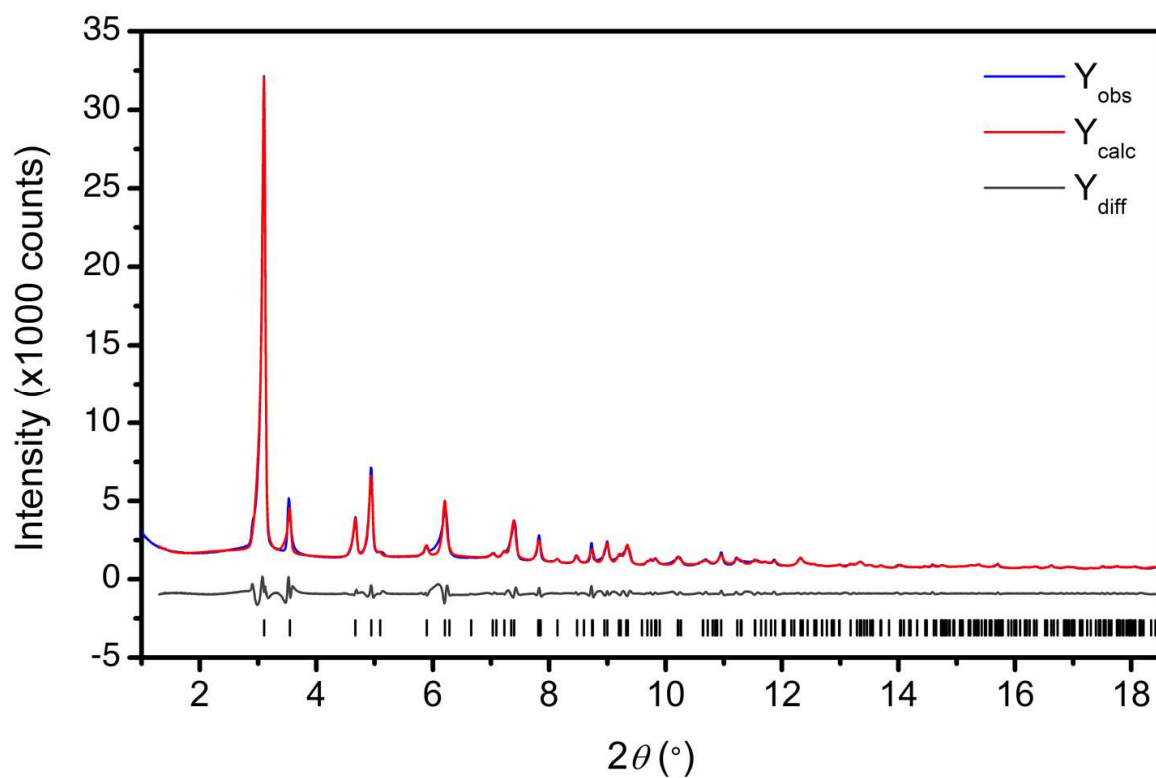
**Figure S18.** Pawley refinement of desolvated Co(bpz) under 70 mbar of $CO_2$ at 257 K from 1.0º to 18.5º. Blue and red lines represent the observed and calculated diffraction patterns, respectively. The gray line represents the difference between observed and calculated patterns, and the black tick marks indicate calculated Bragg peak positions.
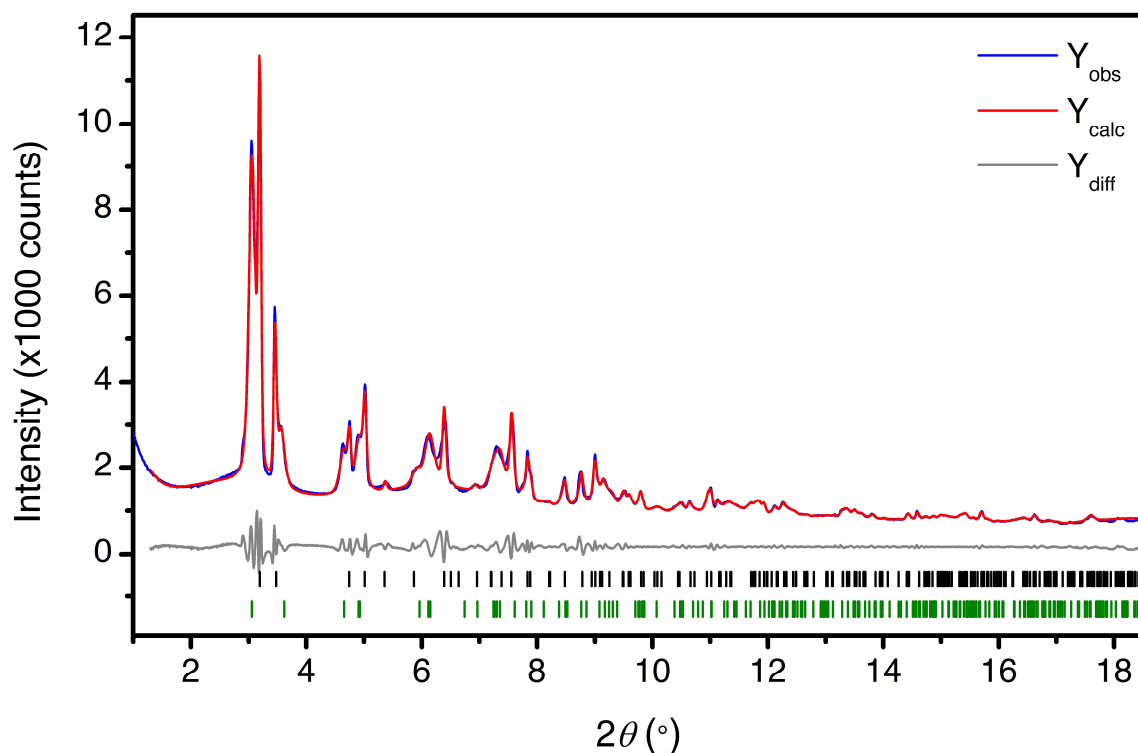
**Figure S19.** Pawley refinement of desolvated Co(bpz) under 70 mbar of $CO_2$ at 247 K from 1.0º to 18.5º. Blue and red lines represent the observed and calculated diffraction patterns, respectively. The gray line represents the difference between observed and calculated patterns, and the black tick marks indicate calculated Bragg peak positions.

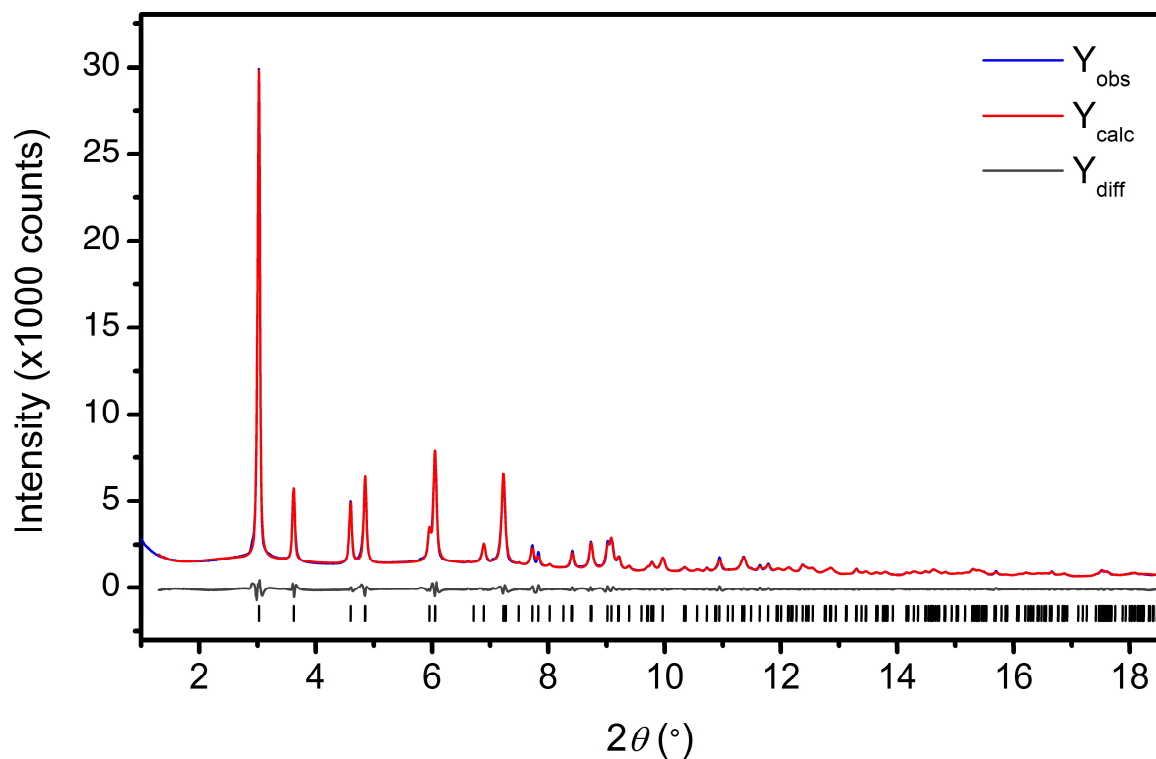**Figure S20.** Pawley refinement of desolvated Co(bpz) under 70 mbar of $CO_2$ at 237 K from 1.0º to 18.5º. Blue and red lines represent the observed and calculated diffraction patterns, respectively. The gray line represents the difference between observed and calculated patterns, and the black tick marks indicate calculated Bragg peak positions.

**Figure S21.** Pawley refinement of desolvated Co(bpz) dosed with 70 mbar of $CO_2$ and cooled to 227 K from 1.0° to 18.5°. Blue and red lines represent the observed and calculated diffraction patterns, respectively. The gray line represents the difference between observed and calculated patterns, and the black tick marks indicate calculated Bragg peak positions. Figures-of-merit (as defined by TOPAS): $R_{wp} = 7.42\%$, $R_p = 4.51\%$, and $R_{exp} = 2.48\%$. The wavelength was 0.45118 Å.
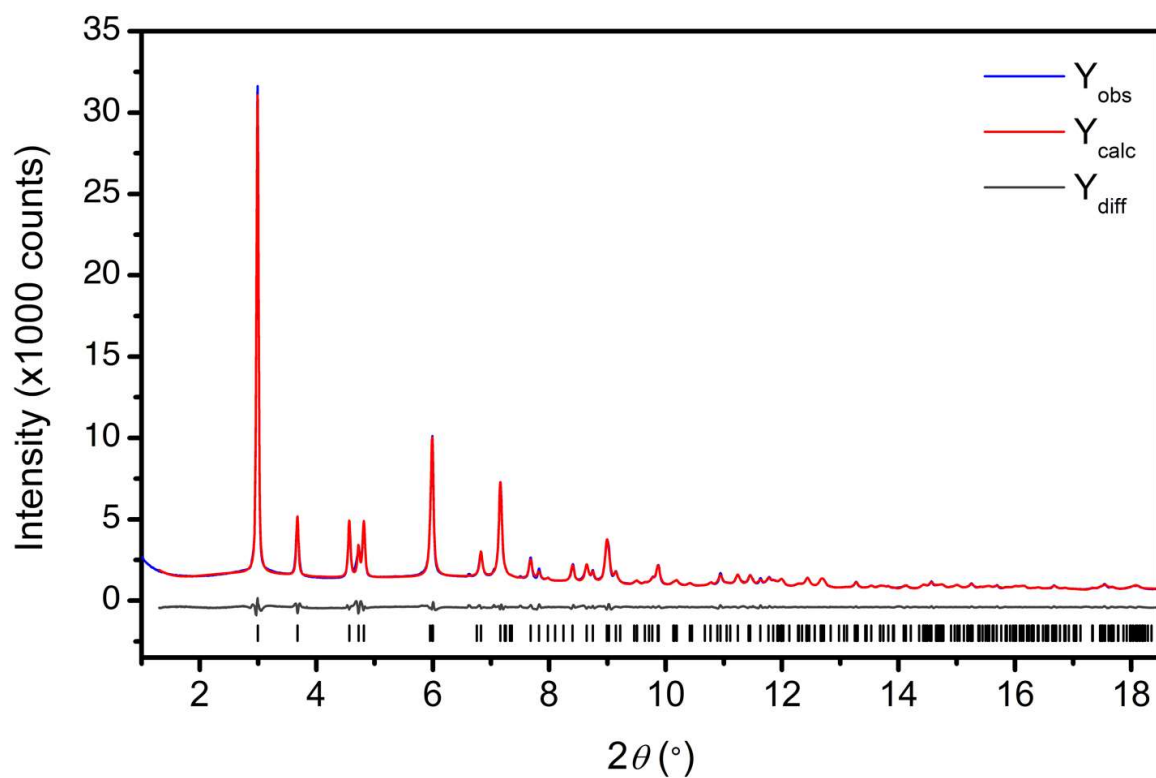
**Figure S22.** Pawley refinement of desolvated Co(bpz) under 70 mbar of $CO_2$ at 217 K from 1.0° to 18.5°. Blue and red lines represent the observed and calculated diffraction patterns, respectively. The gray line represents the difference between observed and calculated patterns, and the black tick marks indicate calculated Bragg peak positions.
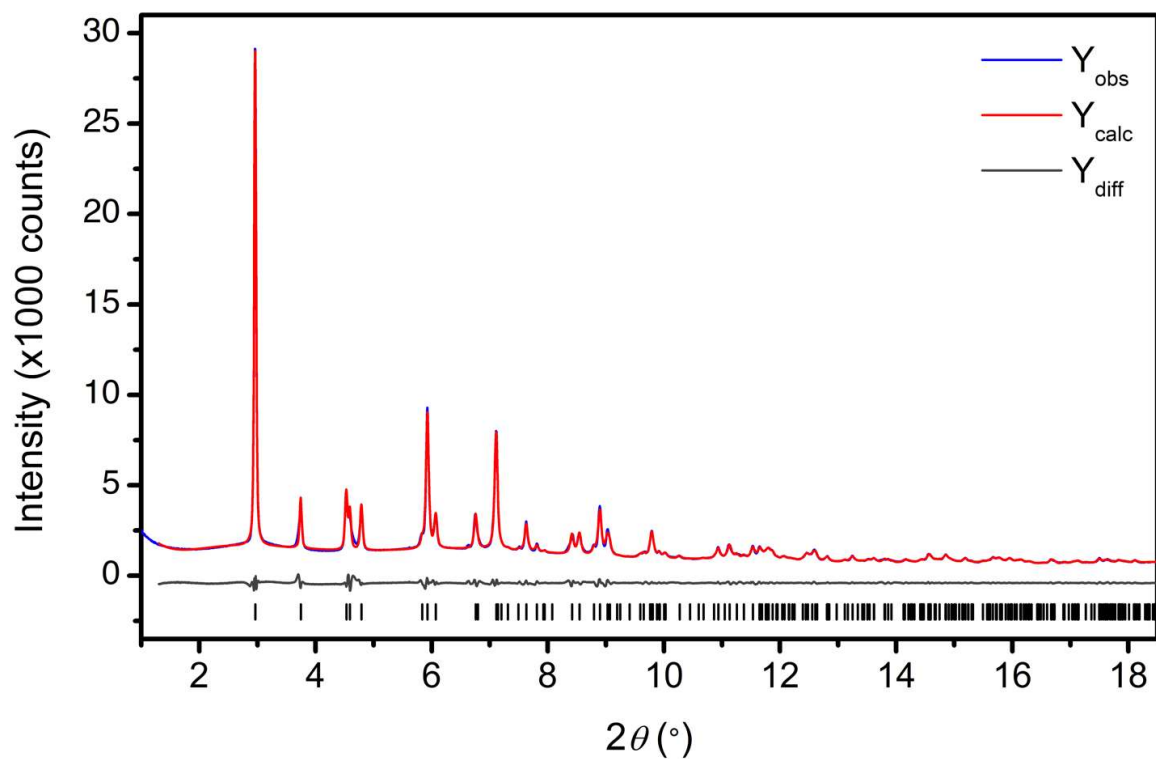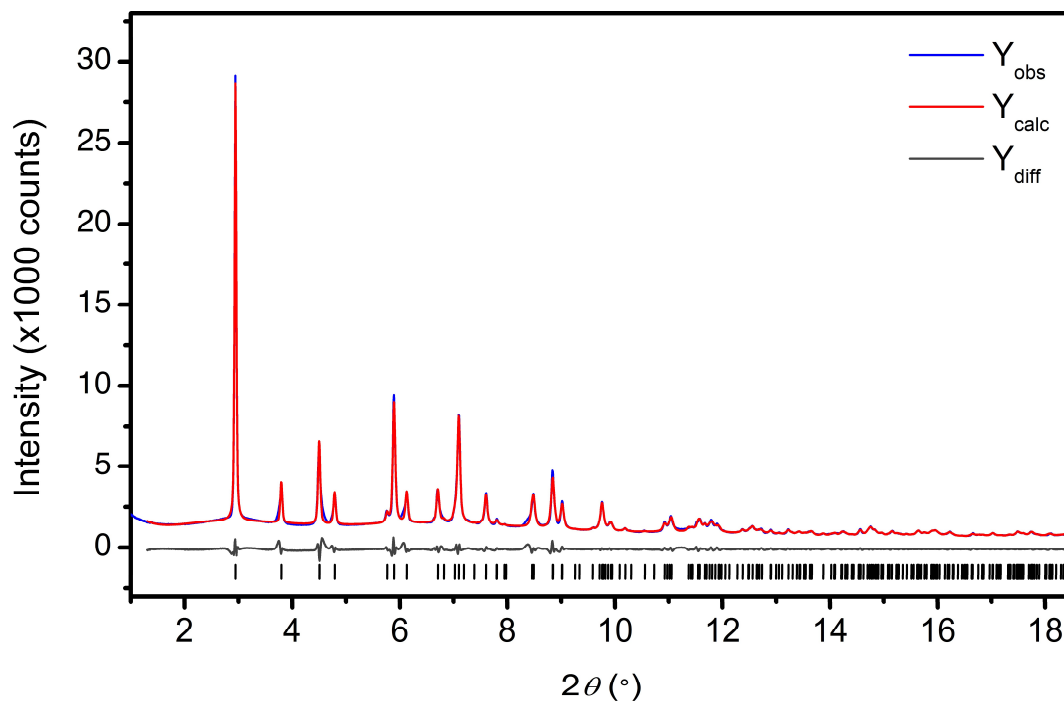
**Figure S23.** Pawley refinement of desolvated Co(bpz) dosed with 70 mbar of $CO_2$ and cooled to 207 K from 1.0° to 18.5°. Blue and red lines represent the observed and calculated diffraction patterns, respectively. The gray line represents the difference between observed and calculated patterns, and the black and green tick marks indicate calculated Bragg peak positions for the two phases (smaller and larger unit cell volumes, respectively). Figures-of-merit (as defined by TOPAS): $R_{wp}$ = 3.86%, $R_p$ = 2.68%, and $R_{exp}$ = 2.36%. The wavelength was 0.45118 Å.

**Figure S24.** Pawley refinement of desolvated Co(bpz) dosed with 70 mbar of $CO_2$ and cooled to 197 K from 1.0° to 18.5°. Blue and red lines represent the observed and calculated diffraction patterns, respectively. The gray line represents the difference between observed and calculated patterns, and the black tick marks indicate calculated Bragg peak positions. Figures-of-merit (as defined by TOPAS): $R_{wp} = 3.13\%$, $R_p = 2.26\%$, and $R_{exp} = 2.48\%$. The wavelength was 0.45118 Å.

**Figure S25.** Pawley refinement of desolvated Co(bpz) under 70 mbar of $CO_2$ at 187 K from 1.0º to 18.5º. Blue and red lines represent the observed and calculated diffraction patterns, respectively. The gray line represents the difference between observed and calculated patterns, and the black tick marks indicate calculated Bragg peak positions.

**Figure S26.** Pawley refinement of desolvated Co(bpz) under 70 mbar of $CO_2$ at 177 K from 1.0º to 18.5º. Blue and red lines represent the observed and calculated diffraction patterns, respectively. The gray line represents the difference between observed and calculated patterns, and the black tick marks indicate calculated Bragg peak positions.

**Figure S27.** Pawley refinement of desolvated Co(bpz) dosed with 70 mbar of $CO_2$ and cooled to 165 K from 1.0º to 18.5º. Blue and red lines represent the observed and calculated diffraction patterns, respectively. The gray line represents the difference between observed and calculated patterns, and the black tick marks indicate calculated Bragg peak positions. Figures-of-merit (as defined by TOPAS): $R_{wp} = 4.37\%$, $R_p = 2.84\%$, and $R_{exp} = 2.47\%$. The wavelength was 0.45118 Å.
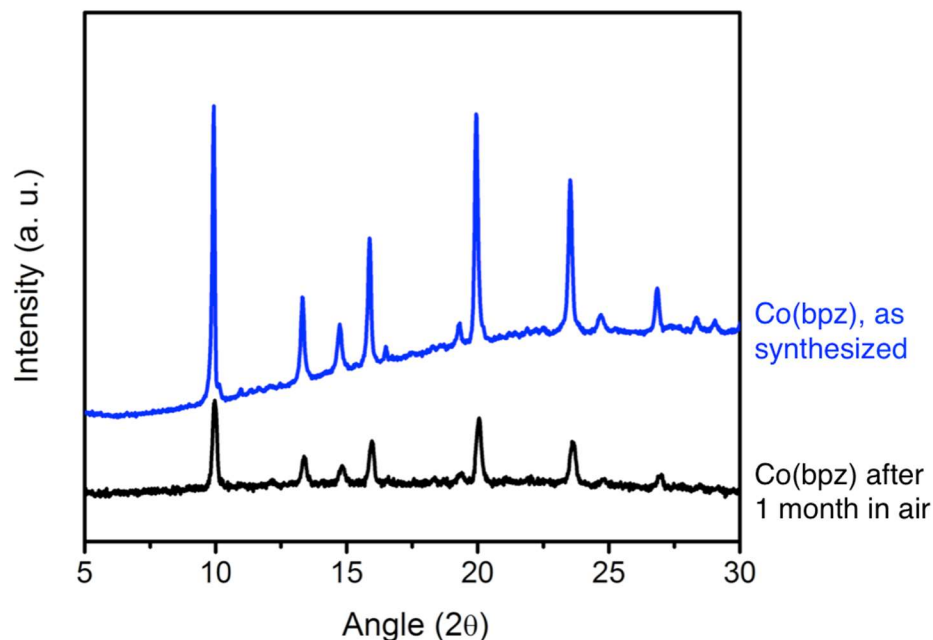
**Figure S28.** Powder X-ray diffraction patterns of Co(bpz) immediately after synthesis (blue) and after storage for one month under air (black). The diffraction patterns are identical, indicating that the material is stable to air and did not lose crystallinity during the course of one month. The higher background for the as-synthesized sample is likely due to X-ray fluorescence from the cobalt present in the sample.
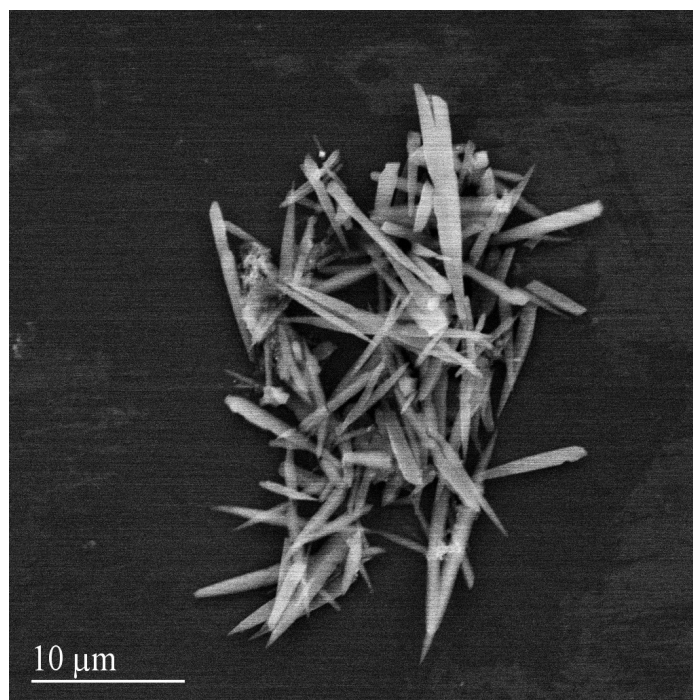


**Figure S29.** Scanning electron micrograph of dichloromethane-solvated Co(bpz).
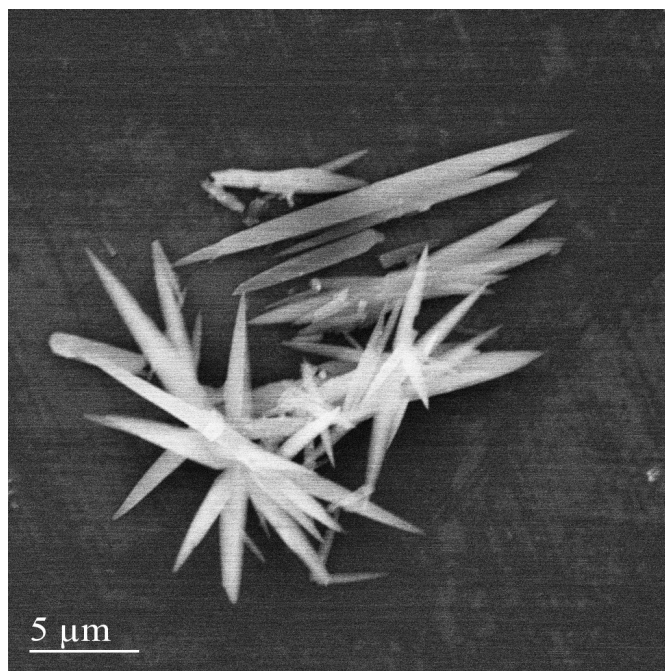
**Figure S30.** Scanning electron micrograph of dichloromethane-solvated Co(bpz).
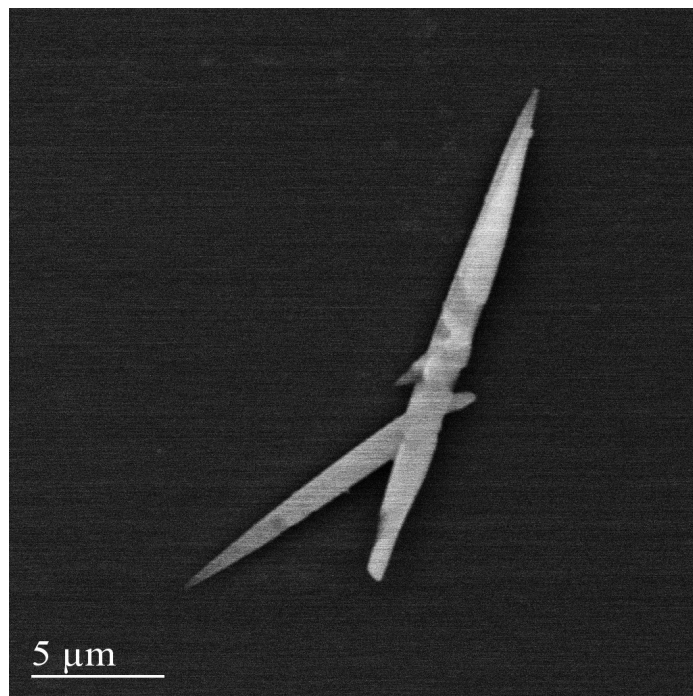


**Figure S31.** Scanning electron micrograph of dichloromethane-solvated Co(bpz).

## Acknowledgements

## References

1. Coelho, A. A. TOPAS-Academic, Version 5 (Coelho Software, 2017).
2. Coelho, A. A. Indexing of Powder Diffraction Patterns by Iterative Use of Singular Value Decomposition. *J. Appl. Cryst.* **2003**, *36*, 86–95.
3. Pawley, G. S. Unit-cell refinement from powder diffraction scans. *J. Appl. Cryst.* **1981**, *14*, 357–361.
4. Andreev, Y. G.; MacGlashan, G. S.; Bruce, P. G. Ab Initio Solution of a Complex Crystal Structure from Powder-Diffraction Data Using Simulated-Annealing Method and a High Degree of Molecular Flexibility. *Phys. Rev. B* **1997**, *55*, 12011–12017.
5. Rietveld, H. M. A Profile Refinement Method for Nuclear and Magnetic Structures *J. Appl. Cryst.* **1969**, *2*, 65–71.
6. Mercury CSD 3.3 (Build RC5), 2013.
7. Coelho, A. A. TOPAS-Academic, Version 4.1 (Coelho Software, 2007).
8. Mason, J. A.; Oktawiec, J.; Taylor, M. K.; Hudson, M. R.; Rodriguez, J.; Bachman, J. E.; Gonzalez, M. I.; Cervellino, A.; Guagliardi, A.; Brown, C. M.; Llewellyn, P. L.; Masciocchi, N.; Long, J. R. Methane Storage in Flexible Metal–Organic Frameworks with Intrinsic Thermal Management. *Nature* **2015**, *527,* 357–361.